Gut Microbiota-Stimulated Innate Lymphoid Cells Support β-defensin 14 Expression in Pancreatic Endocrine Cells Preventing Autoimmune Diabetes

Michela Miani, Julie Le Naour, Emmanuelle Waeckel-Enée, Subash Chand Verma, Marjolene Straube, Patrick Emond, Bernhard Ryffel, Peter van Endert, Harry Sokol, Julien Diana

Gut Microbiota-Stimulated Innate Lymphoid Cells Support β-defensin 14 Expression in Pancreatic Endocrine Cells Preventing Autoimmune Diabetes.

Michela Miani[1], Julie Le Naour[1], Emmanuelle Waeckel-Enée[1], Subash chand Verma[1], Marjolène Straube[2], Patrick Emond[3,4], Bernhard Ryffel[5], Peter van Endert[1], Harry Sokol[2,6,7], Julien Diana[1].

[1]Institut Necker-Enfants Malades (INEM), Institut National de la Santé et de la Recherche Médicale (INSERM), Centre National de la Recherche Scientifique (CNRS), Sorbonne Universités (Paris-Descartes), Paris, France.

[2]Sorbonne Universités, UPMC, Paris 06, École normale supérieure, CNRS, INSERM, APHP Laboratoire des Biomolécules (LBM), Paris, France.

[3]UMR 1253, iBrain, Université de Tours, Inserm, France.

[4]CHRU de Tours, Service de Médecine Nucléaire In Vitro, Tours, France.

[5]Laboratory of experimental and molecular immunology and neurogenetics, UMR 7355 CNRS-University of Orleans, 3B, F-45071 Orleans-Cedex2, France and IDM, Institute of Infectious Disease and Molecular Medicine, University of Cape Town, RSA.

[6]Micalis Institute, Institut National de la Recherche Agronomique (INRA), AgroParisTech, Université Paris-Saclay, Jouy-en-Josas, France.

[7]Department of Gastroenterology, Saint Antoine Hospital, Assistance Publique Hopitaux de Paris, Paris, France.

Corresponding Author and Lead Contact: Dr. Julien Diana, INSERM U1151, Institut Necker-Enfants Malades (INEM), Inserm U1151, Hôpital Necker, 149, rue de Sèvres, 75015 Paris, France; E-mail: julien.diana@inserm.fr

Summary

The gut microbiota is essential for the normal function of the gut immune system and microbiota alterations are associated with autoimmune disorders. However how the gut microbiota prevents autoimmunity in distant organs remains poorly defined. Here we reveal that gut microbiota conditioned-innate lymphoid cells (ILCs) induce the expression of mouse β-defensin 14 (mBD14) by pancreatic endocrine cells preventing autoimmune diabetes in the non-obese diabetic (NOD) mice. MBD14 stimulates, *via* TLR2, IL-4-secreting B cells that induce regulatory macrophages, which in turn induce protective regulatory T cells. The gut microbiota-derived molecules, AHR ligands and butyrate, promote IL-22 secretion by pancreatic ILCs that induces expression of mBD14 by endocrine cells. Dysbiotic microbiota and low-affinity AHR allele explain the defective pancreatic expression of mBD14 observed in NOD mice. Our study reveals a yet unidentified crosstalk between ILCs and endocrine cells in the pancreas that is essential for the prevention of autoimmune diabetes development.

Introduction

Antimicrobial peptides (AMPs) also called host defense peptides, are evolutionarily conserved molecules of the immune system found in almost all plants and animals. AMPs, mainly cathelicidins, defensins and regenerating islet-derived proteins, are mainly expressed at the epithelial surfaces and due to their microbicide ability, AMPs play a critical role in fighting infection and in regulating the microbiota (Bevins and Salzman, 2011; Hancock et al., 2016; Ostaff et al., 2013; Zasloff, 2002; Zhang and Gallo, 2016). In the last decades, the ability of AMPs to modulate pro- and anti-inflammatory immune responses has been increasingly appreciated (Hancock et al., 2016; Zhang and Gallo, 2016). Not surprisingly, dysregulated expression of AMPs has been associated with autoinflammatory and autoimmune diseases such as atherosclerosis, systemic lupus erythematous, rheumatoid arthritis or type 1 diabetes (T1D) (Diana et al., 2013; Frasca and Lande, 2012; Kahlenberg and Kaplan, 2013). Recently, we have revealed the protective role of cathelicidin against autoimmune diabetes in the NOD mouse model. In diabetes-resistant mouse strains, cathelicidin is constitutively expressed by pancreatic endocrine cells and owing to its immunoregulatory abilities, prevents pancreatic inflammation. We have further showed that pancreatic expression of cathelicidin is regulated by gut microbiota-derived metabolites and that, due to dysbiosis in NOD mice, pancreatic expression of cathelicidin is defective allowing the development of autoimmune diabetes (Sun et al., 2015). While the recent literature highlights the role of cathelicidin in autoimmunity, how β-defensins may also modulate autoimmune diseases remains poorly investigated. A recent study demonstrates the protective role of the β-defensin 14 (mBD14) against experimental autoimmune encephalomyelitis (EAE) a mouse model of multiple sclerosis (Bruhs et al., 2016). We hypothesized that mBD14 may also play a role in the development of autoimmune diabetes in NOD mice. Here, we reveal that mBD14 is a part of a complex interplay between the gut

microbiota, innate immune cells and pancreatic endocrine cells preserving immune tolerance in the pancreas and preventing autoimmune diabetes.

Results

Pancreatic endocrine cells express mBD14 in non-autoimmune but not in NOD mice.

β-defensins are known to be expressed by epithelial cells in the gut, skin or lung but their expression in the pancreas remains unknown (Ganz, 2003). Using confocal microscopy, we observed that mBD14 was expressed by pancreatic endocrine cells (glucagon$^+$ α-cells and insulin$^+$ β-cells) with a lower expression in NOD mice compared with BALB/c and C57BL/6 mice (**Figure 1A** and S**1A**). Expression of human β-defensin 3 (hBD3), the orthologue of mBD14, was observed in pancreatic endocrine cells from healthy donors, in accordance with the evolutionary conserved nature of AMPs (**Figure 1B**). Interestingly, the expression of mBD14 mRNA in pancreatic islets was lower in NOD female mice compared with non-autoimmune female mice and lower in female NOD mice compared with male NOD mice (**Figure 1C, D**). These results suggest that mBD14 may play a protective role against autoimmune diabetes since male NOD mice are partially protected against the disease. These data prompted us to investigate whether mBD14 modulates the development of autoimmune diabetes in female NOD mice.

MBD14 is protective against autoimmune diabetes in NOD mice.

We investigated whether administration of mBD14 modulates the development of autoimmune diabetes in NOD mice. RNAseq analysis revealed significant transcriptome changes in pancreatic islets of NOD mice after mBD14 administration. Noticeably, many genes related to inflammation were identified among down-regulated genes in mBD14-treated NOD mice (**Figure S2A-B**). Flow cytometry analysis confirmed the anti-inflammatory effect of mBD14 in pancreatic islets as administration of mBD14 but not of scrambled peptide (scmBD14) reduced the frequency of pancreatic IFNγ$^+$ CD8$^+$ effector T cells specific for the β-cell antigen islet-specific glucose-6-phosphatase catalytic subunit related protein (IGRP)$_{206\text{-}214}$ (**Figure 1E**).

Accordingly, treatment of prediabetic NOD mice with mBD14 but not with scmBD14 reduced the immune infiltration of the pancreatic islets and the incidence of autoimmune diabetes (**Figure S1C and 1F**). Additionally mBD14-treatment of hyperglycemic NOD mice resulted in a transient decrease of their glycaemia (**Figure S1B**). To decipher how mBD14 regulated the diabetogenic immune response, we analyzed pancreatic immune cells from mBD14-treated NOD mice. MBD14 treatment significantly increased the number of B cells and macrophages, while the number of dendritic cells (cDCs) and T cells remained unchanged (**Figure 1G and Figure S1D**). No significant difference was observed in the pancreatic lymph nodes (PLN) or in the spleen (**Figure S1E-F**). But the number of B cells in the PLN had a tendency to increase suggesting that mBD14 may also impact B cells in this organ. Together these data support a protective effect of mBD14 against autoimmune diabetes in NOD mice *via* the regulation of the diabetogenic response.

MBD14 induces pancreatic regulatory B cells.

To decipher the immunoregulatory effect of mBD14, we analyzed pancreatic B cells as their number significantly increased in mBD14-treated NOD mice. Although the precise role of B cells in T1D remains vague, it is believed that cytokine production and auto-antigen presentation by autoreactive B cells to self-reactive T cells play a significant role in the pathogenesis of T1D (Bloem and Roep, 2017). Additionally, Breg cell induction in pancreatic islets dampens the local inflammation and prevents disease development (Boldison and Wong, 2016). We observed that mBD14 treatment induced pancreatic B cell proliferation as demonstrated by increased Ki67 expression (**Figure 2A**) and B cell recruitment likely from PLN as showed by increased expression of CXCL13 mRNA (**Figure S2C**). Functionally, mBD14-induced B cells showed an increased expression of the regulatory molecules IL-4, active transforming growth factor β (TGFβ) (LAP) and Indoleamine 2,3-dioxygenase (IDO)

while IL-10 expression was not significantly increased (**Figure 2B**). About 25% of B cells were double positive for IDO and IL-4 with cells also expressing LAP. The induction of IL-4$^+$ B cells by mBD14 in pancreatic islets was dose-dependent and not observed with scmBD14 (**Figure S2D**), and not observed in the PLN or the spleen (**Figure S2E**). Using an IL-4-neutralizing mAb, we demonstrated that IL-4 was required for the protection against diabetes conferred by mBD14 treatment (**Figure 2C**). Regulatory B (Breg) cells are classically characterized by the expression of CD5 and other surface markers depending on the context studied (Mauri and Menon, 2015). IL-10$^+$ CD138$^+$ plasma cells were also described to be protective against experimental autoimmune encephalomyelitis (EAE)(Fillatreau et al., 2002). Here, IL4$^+$ mBD14-induced B cells expressed CD5, CD1d, B220, CD21 and CD24 but were negative for CD138 (**Figure 2D, E** and **Figure S2F-G**). Next, using *in vitro* system, we wanted to determine the receptor for mBD14 at the surface of pancreatic B cells. *In vitro*, mBD14 induced IL-4 and LAP expression in isolated B cells in a dose dependent manner (**Figure 2F**). Using B cells from *myd88*$^{-/-}$ NOD mice, we found that mBD14 acted *via* TLRs and more particularly *via* the TLR1/2 heterodimer as demonstrated by the use of anti-TLR2 blocking antibody and of the TLR1/2 heterodimer antagonist CU-CTP22 (**Figure 2G**). Noticeably, pancreatic CD5$^+$ B cells expressed a higher level of TLR2 compared with CD5$^-$ B cells, partially explaining why CD5$^+$ B cells were a preferential target for mBD14 (**Figure S2H**). Together our data support that mBD14 targets pancreatic B cells *via* TLR2 inducing the expression of regulatory cytokines.

MBD14-induced B cells promote regulatory macrophages and T cells.

Pancreatic mBD14-induced B cells were characterized by their high expression of IL-4, a cytokine known to drive macrophage polarization to a regulatory phenotype (Mantovani et al., 2007). After mBD14 treatment, we observed an increased frequency of pancreatic macrophages likely due to the increased expression of the macrophage-recruiting chemokines CCL3 and

CCL5 in pancreatic islets (**Figure S3A**). Interestingly mBD14 treatment decreased the ratio between inflammatory $CD11c^+$ $CD206^-$ macrophages and regulatory $CD206^+$ $CD11c^-$ macrophages and this decrease was dependent on IL-4 and B cells as demonstrated by the use of an IL-4-neutralizing mAb and anti-CD20 depleting mAb (**Figure 3A**). Functionally, mBD14 treatment switched the expression of cytokines in pancreatic macrophages from an inflammatory profile (TNFα, IL-12) towards a regulatory profile (IL-4, TGFβ) (**Figure 3B**) and induced the mRNA expression of arginase I and Ym1/Ym2, two markers of regulatory macrophages (**Figure S3A**). *In vitro*, we did not observed a direct effect of mBD14 on bone marrow-derived macrophages (**Figure S3B**) suggesting that the induction of regulatory macrophages by mBD14 was only dependent on IL-4-secreting B cells. DCs, the other main antigen-presenting cells in pancreatic islets were also affected by mBD14 treatment with a reduction of IL-12 expression (**Figure S3C**). Both macrophages and DCs have the potential to induce regulatory T (Treg) cells necessary for a long-term protection against autoimmune diabetes (Tang and Bluestone, 2008). Ten days after mBD14 treatment, the frequency and number of $Foxp3^+$ Treg cells increased in pancreatic islets but not in the PLN or the spleen (**Figure 3C and Figure S3D, E**). Using neutralizing antibodies, we demonstrated that induction of Treg cells by mBD14 was dependent on IL-4 and TGFβ, two cytokines produced by mBD14-induced B cells and macrophages (**Figure 3D**). To determine the contribution of each cell type in Treg cell induction we used an *in vitro* system. Isolated pancreatic myeloid cells ($CD11b^+$ cells) or B cells ($CD19^+$ cells) from vehicle- or mBD14-treated NOD mice were cultured with monoclonal naïve ($CD62L^+$) autoreactive BDC2.5 $CD4^+$ T cells devoid of Treg cells ($CD25^-$). Myeloid cells but not B cells were able to induce Treg cells regardless their source. However, myeloid cells from mBD14-treated NOD mice had a significantly higher potency to induce Treg cells compared to their counterparts from vehicle-treated NOD mice (**Figure 3E and Figure S3F**). We did not observe an induction of a regulatory phenotype in BDC2.5 T cells

cultured alone with mBD14 excluding a direct effect of the peptide on these T cells (**Figure S3G**). Together, our data support that mBD14 induces an immunoregulatory cascade in pancreatic islets from B cells to Treg cells.

IL-22 promotes pancreatic expression of mBD14

We next sought to determine the pathway governing pancreatic expression of mBD14 and why this pathway was defective in NOD mice. In the gut, but also in other tissues including the pancreas, IL-22 has emerged as a key cytokine in tissue homeostasis partially through its ability to promote the production of AMPs (Aujla et al., 2008; Hill et al., 2013; Liang et al., 2006; Mulcahy et al., 2016; Sonnenberg et al., 2012; Wolk et al., 2004). The IL-22 receptor is highly expressed by pancreatic islets and β-cells (Shioya et al., 2008; Wolk et al., 2004), and we hypothesized that IL-22 may induce mBD14 expression in pancreatic endocrine cells. We observed that IL22 mRNA expression was reduced in pancreatic islets from female NOD mice compared with female non-autoimmune mice (**Figure 4A**) and male NOD mice (**Figure S4A**). The IL-22 level in the serum was also reduced in female NOD mice (**Figure S4B**). Importantly the administration of IL-22Fc to NOD mice induced the expression of mBD14 mRNA in pancreatic islets (**Figure 4B**). *In vitro,* rIL-22 induced mBD14 by targeting directly mouse and human pancreatic islets (**Figure 4C, D**). Moreover, rIL-22 induced the expression of mBD14 in the Min6 β-cell line (**Figure S4C**). As previously described (Hill et al., 2013; Kinnebrew et al., 2012), IL-22Fc also stimulated the expression of the protective AMP Reg3γ in pancreatic islets and ileum (**Figure S4D, E**). Together, these data support that IL-22 induces the expression of mBD14 by pancreatic endocrine cells.

Type 3 innate lymphoid cells are the main source of IL-22 in pancreatic islets.

Both type 3 innate lymphoid cells (ILC3s) and conventional T cells can produce IL-22 (Sabat et al., 2014). By flow cytometry, we investigated the ILC population in pancreatic islets from NOD, C57BL/6 and BALB/c mice. ILCs ($CD127^+$ $CD90^+$ Lin^-) were observed in pancreatic islets of all mouse strains in equal number (**Figure 4E**). We confirmed these data using *rag*$^{-/-}$ mice to exclude a potential contamination with conventional T cells in our gating strategy (**Figure S4F**). Analyzing pancreatic ILC subtypes, we observed a reduction in the frequency of RORγt$^+$ ILC3s in NOD mice compared with non-autoimmune mice (**Figure 4F and Figure S4G**). Accordingly, the expression of IL-22 by pancreatic ILCs was reduced in NOD mice compared with non-autoimmune mice (**Figure 4G and S4J**). Conventional α/β and γ/δ T cells did not significantly expressed IL-22 in pancreatic islets from all mouse strains (**Figure S4H-J**). Using confocal microscopy, we observed the presence of IL-22$^+$ CD5$^-$ cells and IL-22$^-$ CD5$^+$ cells inside the pancreatic islets of C57BL/6 mice (**Figure 4H and S5A**). To confirm that only ILCs and not T cells were needed as an IL-22 source to induce mBD14 in the pancreatic islets, we treated C57BL/6 *rag*$^{-/-}$ mice with the IL-22 inducer IL-23. We observed that IL-23 efficiently increased mRNA expression of IL-22 and mBD14 in the pancreatic islets and ileum of these T-cell deficient mice (**Figure S5B-E**). The reduced frequency of ILC3s in NOD mice was not observed in pancreatic or mesenteric LN (**Figure S6A-B**). Furthermore, despite a high frequency of ILC3s in pancreatic or mesenteric LN of NOD mice, ILCs in these organs did not expressed higher level of IL-22 compared with non-autoimmune strains, but rather expressed significantly higher level of IFNγ and TNFα (**Figure S6C-D**). Together our data support that IL-22 production was defective in NOD mice and that pancreatic ILC3s were the source of IL-22 promoting mBD14 expression in pancreatic islets of non-autoimmune mice.

Gut microbiota controls IL-22 and mBD14 expression in pancreatic islets.

It is recognized that microbiota controls the production of IL-22 by ILC3s in the gut (Klose and Artis, 2016). To evaluate how gut microbiota may control IL-22 and consequently mBD14 expression in pancreatic islets, we treated BALB/c mice with a cocktail of broad-spectrum antibiotics (ABX) to reduce the gut microbiota. As described in the skin (Zanvit et al., 2015), ABX-treatment decreased IL-22 protein level in the serum and mRNA expression of IL22 in pancreatic islets (**Figure 5A, B**). In parallel, ABX-treatment decreased the expression of mBD14 mRNA in pancreatic islets suggesting that the gut microbiota controlled the expression of mBD14 in pancreatic islets *via* the induction of IL-22 (**Figure 5C**). To confirm these data, we performed gut microbiota-transfer experiments. Expression of mBD14 and IL22 mRNA was increased in pancreatic islets from NOD mice that received gut microbiota from BALB/c mice or C57BL/6 mice compared with NOD mice supplied with NOD gut microbiota (**Figure 5D and S7A**). Together, these data support that the gut microbiota controls the expression of mBD14 in pancreatic islets *via* IL-22 induction.

Gut microbiota drives pancreatic IL-22 expression *via* AHR ligands and IL-23.

In the gut, microbiota controls the expression of IL-22 by ILC3s *via* different pathways (Zhou, 2016). Specific bacteria species produce aryl hydrocarbon receptor (AHR) ligands that directly activate ILC3s to produce IL-22. Other bacteria species produce metabolites that promote IL-23 secretion by intestinal phagocytes and IL-23 activates ILC3s to produce IL-22. Consequently, we hypothesized that one of these pathways or both may be at play in pancreatic islets to stimulate the production of IL-22. To evaluate the ability of AHR ligand to stimulate mBD14 expression in pancreatic islets, we administrated the AHR ligand 6-Formylindolo-[3,2-b]-carbazole (FICZ) to BALB/c mice. FICZ administration induced mRNA expression of Cyp1a1 in pancreatic islets confirming the activation of AHR^+ cells (**Figure 6A**) and increased the expression of IL22 and mBD14 mRNA in pancreatic islets (**Figure 6B, C**). A similar

induction of mBD14 was observed after injection of the AHR ligand indole-3-aldehyde, a tryptophan metabolite naturally produced by the gut microbiota (**Figure 6C**). As systemic AHR ligand administration may induce mBD14 in pancreatic islets *via* indirect pathways, we treated isolated pancreatic islets *in vitro* with FICZ and we observed an increased expression of Cyp1a1, IL22 and mBD14 mRNAs (**Figure 6D-F**). The induction of pancreatic mBD14 by FICZ was dependent on IL-22 as demonstrated by the use of neutralizing mAb (**Figure 6F**) and by the fact that FICZ did not induce mBD14 expression in Min6 β-cell line excluding a direct role of AHR ligand on β-cells (**Figure 6G**). Using a reporter assay, we failed to observe a significant defect in AHR ligand activity in the feces or the serum of NOD mice compared with non-autoimmune mice (**Figure 6H, I**). Similarly, using mass spectrometry, we did not detect significant difference in the concentration of various AHR ligands in the feces or the serum of NOD mice compared with non-autoimmune mice (**Figure S7C**). These data made unlikely that a defective AHR ligand production in NOD mice may explain the defect in mBD14 expression in pancreatic islets. Nevertheless, NOD strain expresses a low affinity AHR^d allele contrary to BALB/c or C57BL/6 strains carrying the AHR^b allele (Kerkvliet et al., 2009; Okey et al., 2005). Accordingly, by analyzing the expression of Cyp1a1 mRNA, we found that pancreatic islet cells from NOD mice were hyporesponsive to FICZ compared with BALB/c islet cells (**Figure 6J**). These data support that AHR ligands stimulated IL-22-secreting AHR^+ cells in pancreatic islets inducing mBD14 expression but in NOD mice, due to the presence of a low affinity AHR allele, the level of AHR ligands may be insufficient to promote IL-22 and mBD14 expression. Then, we evaluated how IL-23 may also be implicated in the induction of mBD14 in pancreatic islets. Expression of IL23 mRNA was reduced in pancreatic islets from NOD mice compared with BALB/c and C57BL/6 mice (**Figure 7A**) and IL23 mRNA expression was increased in pancreatic islets from NOD mice that received gut microbiota from BALB/c mice or C57BL/6 mice compared with NOD mice supplied with NOD gut microbiota (**Figure S7B**). Flow

cytometry analysis of pancreatic phagocytes confirmed a defective IL-23 expression in NOD mice compared with non-autoimmune strains (**Figure 7B**). In non-autoimmune mice, pancreatic IL-23 expression was mainly supported by macrophages (**Figure S7D**). Administration of rIL-23 to BALB/c mice increased the level of IL-22 in the serum associated with an increased expression of IL22 and mBD14 mRNA in pancreatic islets (**Figure 7C-E**). Then we attempted to determine why pancreatic phagocytes failed to produce IL-23 in NOD mice. A recent study and our present data (**Figure S7E**) demonstrated the effect of butyrate, a microbiota-derived metabolite, in upregulating IL-23 expression in DCs and macrophages (Berndt et al., 2012). Additionally, our previous study demonstrated that female NOD mice harbored reduced level of butyrate in the serum and the gut compared with non-autoimmune mice (Sun et al., 2015). Thus, we hypothesized that butyrate may stimulate the expression of IL-23 by pancreatic phagocytes and a defective production of butyrate in NOD mice may lead to reduced expression of pancreatic IL-23. By 16s rDNA sequencing from feces of NOD, BALB/c and C57BL/6 mice, we observed that gut microbiota in NOD mice harbored a higher Bacteroidetes/Firmicutes ratio with a lower abundance of Clostridiales Lachnospiraceae, Ruminococcaceae and Erysipelotrichaceae (**Figure 5E-G**). These bacteria families are butyrogenic (Riviere et al., 2016) and their low abundance in NOD mice is in line with the low level of butyrate observed in this strain. Administration of butyrate to BALB/c mice increased the level of IL-23 in the serum and the expression of IL23, IL22 and mBD14 mRNA in pancreatic islets (**Figure 7F-I**), however we failed to observe a significant increase in the expression of mBD14 mRNA in butyrate-treated NOD mice (**Figure S7F**). *In vitro*, butyrate directly stimulated pancreatic islet cells to induce IL23, IL22 and mBD14 mRNA expression (**Figure 7J-L**). This induction of mBD14 by butyrate was dependent on IL-22 as demonstrated by the use of neutralizing mAb (**Figure 7L**). *In vivo*, we observed that butyrate increased the expression of IL-23 by pancreatic phagocytes (**Figure 7M**). Since butyrate failed to induce

mBD14 expression in Min6 β-cell line (**Figure S7G**), we conclude that butyrate induced the expression of mBD14 in pancreatic islets *via* the stimulation of IL-23^{+} phagocytes.

Discussion

The immunomodulatory role of AMPs is increasingly recognized and their involvement in the immunopathology of autoimmune diseases is progressively identified (Kahlenberg and Kaplan, 2013; Mansour et al., 2014). Many studies have revealed the deleterious role of cathelicidin in autoinflammatory and autoimmune diseases including atherosclerosis, small vessel vasculitis, psoriasis and systemic lupus erythematous (Gupta and Kaplan, 2016; Kahlenberg and Kaplan, 2013; Pinegin et al., 2015). In sterile condition, cathelicidin can be aberrantly expressed in the tissues by infiltrating neutrophils stimulating the uncontrolled production of type I IFNs, which are important contributors to autoimmunity (Hall and Rosen, 2010). We have shown that this pathway is also at play during the initiation of autoimmune diabetes in NOD mice (Diana et al., 2013), however we have further demonstrated that cathelicidin may be also protective against autoimmune diabetes (Sun et al., 2015). Indeed, in non-autoimmune-prone mice but not in NOD mice, cathelicidin is produced by pancreatic endocrine cells and this endocrine cathelicidin exerts an immunoregulatory effect on macrophages thereby preserving immune tolerance in the pancreas. Conversely, a recent study shows that the cathelicidin-like peptide FhHDM-1 from the helminth *Fasciola hepatica* regulates inflammatory macrophages, thus dampening the development of diabetes in NOD mice and the severity of EAE, a mouse model of multiple sclerosis (Lund et al., 2016). Collectively, these observations indicate that cathelicidin aberrantly produced from neutrophils is deleterious, while cathelicidin constitutively produced by non-immune cells or exogenous cathelicidin is protective against autoimmune diabetes. These opposite effects of cathelicidin from different cellular source may be due to distinct post-translational modifications which affect its function (Wang, 2012).

Like cathelicidin, β-defensins exert diverse immunomodulatory activities including receptor-mediated chemotaxis or modulation of immune cells *via* TLR regulating both innate and adaptive immunity (Lehrer, 2004; Semple and Dorin, 2012). Studies in the Dorin laboratory of

hBD3 have demonstrated that this defensin inhibits the production of pro-inflammatory cytokines by LPS-primed macrophages *in vitro* and reduces the level of pro-inflammatory cytokines in the serum of LPS-treated mice when administrated *in vivo* (Semple et al., 2011; Semple et al., 2010). Studies from the group of Schwarz have shown the ability of mBD14 to induce Treg cells *in vitro* and *in vivo*, reducing the severity of EAE (Bruhs et al., 2016; Navid et al., 2012). Our present study reveals the direct effect of mBD14 on B cells *via* the TLR1/2 heterodimer that is highly expressed on pancreatic $CD5^+$ B cells. Consistent with our finding, hBD3 activates human monocytes *via* the TLR1/2 heterodimer (Funderburg et al., 2007). Consequently, we cannot totally rule out a direct effect of mBD14 on pancreatic TLR2-expressing phagocytes. Together, the literature and our data support that β-defensins exert immunomodulatory function on different immune cell types ensuring an efficient protection against tissue inflammation and autoimmunity.

Our data support that the protective role of mBD14 against autoimmune diabetes is mediated by induction of IL-4-producing B cells. In line with our results, transgenic expression of IL-4 by pancreatic β-cells efficiently prevents the development of diabetes in NOD mice (Mueller et al., 1996). Using B cell-deficient NOD mice and depleting CD20 antibody, the pathogenic effect of B cells in autoimmune diabetes has been demonstrated (Xiu et al., 2008; Yang et al., 1997). However, various Breg subtypes play a protective role against several immune-related diseases including systemic lupus erythematous, rheumatoid arthritis and autoimmune diabetes (Rosser and Mauri, 2015). Reconciling these observations, the protective effect of B cell depletion against autoimmune diabetes is associated with the induction of IL-10-producing Breg cells in the reconstituted B cell population and the subsequent induction of Treg cells (Di Caro et al., 2014).

We show that IL-22 stimulates pancreatic β-cells to express mBD14 and that IL-22 expression is defective in pancreatic islets of NOD mice. IL-22 is known to induce AMPs including β-

defensins in different tissues (*e.g.* the gut, skin and lung) preventing tissue damage (Aujla et al., 2008; Lindroos et al., 2011; Mulcahy et al., 2016; Wolk et al., 2006; Zheng et al., 2008). Pancreatic β-cells highly express IL-22R (Shioya et al., 2008) and IL-22 is protective against metabolic disorders by improving β-cell proliferation and function and by decreasing inflammation (Hasnain et al., 2014; Wang et al., 2014). Additionally, IL-22 stimulates the expression of the AMPs Reg2 and Reg3 by pancreatic acinar cells preventing tissue damage in a mouse model of pancreatitis (Aggarwal et al., 2001; Xue et al., 2012). In NOD mice, IL-22 promotes the expression of Reg1 and Reg2 by β-cells preventing β-cell loss in an autocrine manner (Hill et al., 2013). Together, IL-22 induces different AMPs in pancreatic islets promoting β-cell function, regulating inflammation and preventing autoimmune response. The therapeutic use of IL-22 may be of interest against autoimmune diabetes. However, *IL22*$^{-/-}$ NOD mice did not display an increased incidence of autoimmune diabetes (Ishigame et al., 2013) but as showed here, NOD mice are characterized by a constitutively low level of pancreatic IL-22 so that genetic complete abrogation may not have a significant impact on the development of the disease. A recent study shows that IL-22 treatment of prediabetic NOD mice does not reduced the incidence of diabetes (Borg et al., 2017). However, as mentioned by the authors, a more pronounced effect may be obtained by increasing the dose, the frequency of administration and by the use of a more metabolically stable Fc-based fusion protein as used against metabolic diseases (Wang et al., 2014) and in our present study. Finally, the endogenous production of the neutralizing IL-22 binding protein may limit the therapeutic use of IL-22 at a lower dose (Martin et al., 2014).

We reveal for the first time the presence of IL-22-secreting ILC3s within pancreatic islets and their defect in NOD mice. In a mouse-model of pancreatitis, AHR-reactive conventional T cells are a source of IL-22 in the whole pancreas (Xue et al., 2012); however, in the pancreatic islets we observe that α/β or γ/δ T cells did not express significant levels of IL-22. The role of ILCs

in autoimmune diseases is an emerging field of research and to our knowledge, the role of ILCs in autoimmune diabetes remains unknown. A deleterious role of IFNγ-producing ILC1s has been proposed in inflammatory bowel diseases while IL-17-producing ILC3s may participate to rheumatic diseases, psoriasis or multiple sclerosis (Shikhagaie et al., 2017). As autoimmune diabetes is not an IL-17-mediated disease (Bedoya et al., 2013), and due to the protective nature of IL-22, pancreatic ILC3s may play a protective role against autoimmune diabetes. Interestingly despite a high number of ILC3s, ILCs in PLN or MLN of NOD mice did not expressed high level of IL-22, but rather expressed significantly levels of IFNγ and TNFα. These data support that the inflammatory environment in the PLN and MLN in NOD mice may influence the cytokine expression of ILCs towards an inflammatory profile regardless of the subtype of ILCs as already described in the gut (Melo-Gonzalez and Hepworth, 2017).

Finally, we show that the expression of IL-22 in pancreatic islets is under the control of the gut microbiota-derived molecules AHR ligands and butyrate. NOD mice such as the DBA/2 strain carry a low affinity *AHR*^{d} genotype contrary to BALB/c or C57BL/6 mice carrying the *AHR*^{b} allele. Consequently, *AHR*^{d} mice require at least a tenfold higher dose of AHR ligand than *AHR*^{b} mice to induce the same effects (Kerkvliet et al., 2009; Okey et al., 2005). These studies and our data support that AHR^{+} cells in NOD mice are hyporesponsive to endogenous AHR ligands. Nevertheless, treatment of NOD mice with high dose of AHR ligand reduces insulitis and the incidence of diabetes *via* the induction of regulatory AHR^{+} DCs and Treg cells (Kerkvliet et al., 2009). The anti-inflammatory effect of AHR ligands is also mediated by the induction of IL-22 in various tissues including the gut, lung and pancreas (Qiu et al., 2012; Simonian et al., 2010; Xue et al., 2012). Together, our data and the literature support a protective role for AHR-dependent IL-22 expression in the pancreas *via* the induction of AMPs promoting β-cell regeneration and controlling inflammation.

As described in the gut (Abraham and Cho, 2009), we show that IL-23 induces IL-22 expression by ILC3s in pancreatic islets. We observed that IL-23 expression is reduced in pancreatic islets of NOD mice as described in the serum of T1D patients (Roohi et al., 2014). Under the influence of gut microbiota derived factors, resident intestinal phagocytes secrete IL-23 inducing, *via* IL-22, the expression of AMPs by epithelial cells (Caballero and Pamer, 2015; Honda and Littman, 2016). Here, we demonstrate that butyrate, a short chain fatty acid classically produced by Clostridia species in the gut microbiota, stimulates the expression of IL-23 by pancreatic phagocytes as previously described (Berndt et al., 2012). We have previously demonstrated that NOD mice harbor a reduced level of circulating butyrate (Sun et al., 2015) and we presently show that the gut microbiota of NOD mice is defective in butyrogenic bacteria confirming previous reports in NOD mice and consistent with findings in children with β-cell autoimmunity (Brown et al., 2016; de Goffau et al., 2013; Endesfelder et al., 2016; Giongo et al., 2011). Together, these data support that butyrate stimulates the production of immunoregulatory AMPs by pancreatic endocrine cells preventing autoimmune diabetes. A recent study also demonstrated the protective role of butyrate against autoimmune diabetes in NOD mice through the expansion of colonic and splenic Treg cells (Marino et al., 2017). Considering the role of butyrate in promoting gut integrity and immune tolerance (Rooks and Garrett, 2016), this gut microbiota-derived metabolite appears as an attractive therapeutic candidate against T1D. Our studies and the literature highlight the beneficial relationships between the pancreas and the gut and this increasing knowledge should lead to identification of new approaches for the treatment of T1D (Tilg and Adolph, 2017).

Limitation of the Study

Our study describes a complex interplay between innate immune cells, pancreatic endocrine cells and the intestinal microbiota participating to the prevention of autoimmune diabetes in

NOD mice. Our data support that gut microbiota-stimulated ILCs, *via* the production of IL-22, promote the expression of immunoregulatory mBD14 by pancreatic endocrine cells. As the number of pancreatic ILCs is low, it would be important to confirm the presence of IL-22-producing ILCs into the pancreatic islets using reporter mice. The role of ILCs in autoimmune diseases is emerging with both protective and deleterious roles described. To strengthen the protective role of pancreatic ILCs against autoimmune diabetes, transfer experiments would be helpful, although these experiments may be challenging due to the difficulty to obtain a sufficient number of ILCs from donor mice. Our group and others have described various pathways used by the gut microbiota to prevent autoimmune diabetes. Before transfer these findings to the clinic, it would be important to determine the relative importance of each of these pathways in the prevention of the disease. Finally, as the well-characterized microbiome of laboratory mouse strain differs from human microbiome continuously facing environmental factors, it is critical to perform human studies to translate our findings to the human disease and envisage future therapies based on our conclusions.

STAR METHODS

Detailed methods are provided in the online version of this paper and include the following:

- KEY RESOURCES TABLE
- CONTACT FOR REAGENT AND RESOURCE SHARING
- EXPERIMENTAL MODEL DETAILS
    - Mice and treatments
    - Spontaneous diabetes incidence
- METHOD DETAILS
    - Preparation of pancreatic islets
    - RT-qPCR

SUPPLEMENTAL INFORMATION

Supplemental Information includes eleven figures.

ACKNOWLEDGMENTS

The authors greatly acknowledge Valérie Gaboriau-Routhiau (Inserm U1163, France), Marie Cherrier (Inserm U1151, France), Gaetan Barbet (Cornell University, USA) and Nicolas Serafini (Inserm U668, France) for fruitful discussions. The authors acknowledge Antoine Lefevre from the PST facility “Analyse des Systèmes Biologiques” (Tours, France). The authors acknowledge the SFR Necker facilities including Meriem Garfa-Traoré and Nicolas Goudin of the Imaging Facility, Christine Bole of the genomics facility, Nicolas Cagnard of the

bioinformatics facility and the team of the mouse facility (Hamburger building). This work was supported by funds from: Peter van Endert received funding from grants from Fondation pour la Recherche Médicale (DEQ20130326539), Idex Sorbonne Paris Cité, Aide aux Jeunes Diabétiques. Harry Sokol received funding from the European Research Council (ERC) under the European Union's Horizon 2020 research and innovation program (ERC-2016-StG-71577). Julien Diana received funding from The Juvenile Diabetes Research Foundation (JDRF)-SRA (2-SRA-2015-73-Q-R), the European Foundation for the Study of Diabetes (EFSD)/Lilly (94169) and the Association Française des Femmes Diabètiques (AFFD).

AUTHOR CONTRIBUTIONS

MM designed, performed and analyzed experiments, with general assistance of JL, EWE and SV for confocal microscopy, histology and cell culture. BR provided the *IL22*$^{-/-}$ C57BL/6 mice. PE performed the mass spectrometry experiments. MS and HS performed gut microbiota analysis and AHR ligand analysis. PvE and HS provide intellectual inputs. JD designed the project, performed experiments, interpreted data and wrote the paper.

DECLARATION OF INTERESTS

The authors declare no competing interests.

REFERENCES

Abraham, C., and Cho, J.H. (2009). IL-23 and autoimmunity: new insights into the pathogenesis of inflammatory bowel disease. Annu Rev Med *60*, 97-110.

Aggarwal, S., Xie, M.H., Maruoka, M., Foster, J., and Gurney, A.L. (2001). Acinar cells of the pancreas are a target of interleukin-22. J Interferon Cytokine Res *21*, 1047-1053.

Aujla, S.J., Chan, Y.R., Zheng, M., Fei, M., Askew, D.J., Pociask, D.A., Reinhart, T.A., McAllister, F., Edeal, J., Gaus, K., *et al.* (2008). IL-22 mediates mucosal host defense against Gram-negative bacterial pneumonia. Nat Med *14*, 275-281.

Bedoya, S.K., Lam, B., Lau, K., and Larkin, J., 3rd (2013). Th17 cells in immunity and autoimmunity. Clin Dev Immunol *2013*, 986789.

Berndt, B.E., Zhang, M., Owyang, S.Y., Cole, T.S., Wang, T.W., Luther, J., Veniaminova, N.A., Merchant, J.L., Chen, C.C., Huffnagle, G.B., and Kao, J.Y. (2012). Butyrate increases IL-23 production by stimulated dendritic cells. Am J Physiol Gastrointest Liver Physiol *303*, G1384-1392.

Bevins, C.L., and Salzman, N.H. (2011). Paneth cells, antimicrobial peptides and maintenance of intestinal homeostasis. Nat Rev Microbiol *9*, 356-368.

Bloem, S.J., and Roep, B.O. (2017). The elusive role of B lymphocytes and islet autoantibodies in (human) type 1 diabetes. Diabetologia *60*, 1185-1189.

Boldison, J., and Wong, F.S. (2016). Immune and Pancreatic beta Cell Interactions in Type 1 Diabetes. Trends Endocrinol Metab *27*, 856-867.

Borg, D.J., Wang, R., Murray, L., Tong, H., Steptoe, R.J., McGuckin, M.A., and Hasnain, S.Z. (2017). The effect of interleukin-22 treatment on autoimmune diabetes in the NOD mouse. Diabetologia.

Brown, K., Godovannyi, A., Ma, C., Zhang, Y., Ahmadi-Vand, Z., Dai, C., Gorzelak, M.A., Chan, Y., Chan, J.M., Lochner, A., *et al.* (2016). Prolonged antibiotic treatment induces a diabetogenic intestinal microbiome that accelerates diabetes in NOD mice. The ISME journal *10*, 321-332.

Bruhs, A., Schwarz, T., and Schwarz, A. (2016). Prevention and Mitigation of Experimental Autoimmune Encephalomyelitis by Murine beta-Defensins via Induction of Regulatory T Cells. J Invest Dermatol *136*, 173-181.

Caballero, S., and Pamer, E.G. (2015). Microbiota-mediated inflammation and antimicrobial defense in the intestine. Annu Rev Immunol *33*, 227-256.

Caporaso, J.G., Kuczynski, J., Stombaugh, J., Bittinger, K., Bushman, F.D., Costello, E.K., Fierer, N., Pena, A.G., Goodrich, J.K., Gordon, J.I., *et al.* (2010). QIIME allows analysis of high-throughput community sequencing data. Nat Methods *7*, 335-336.

de Goffau, M.C., Luopajarvi, K., Knip, M., Ilonen, J., Ruohtula, T., Harkonen, T., Orivuori, L., Hakala, S., Welling, G.W., Harmsen, H.J., and Vaarala, O. (2013). Fecal microbiota composition differs between children with beta-cell autoimmunity and those without. Diabetes *62*, 1238-1244.

Di Caro, V., Phillips, B., Engman, C., Harnaha, J., Trucco, M., and Giannoukakis, N. (2014). Involvement of suppressive B-lymphocytes in the mechanism of tolerogenic dendritic cell reversal of type 1 diabetes in NOD mice. PLoS One *9*, e83575.

Diana, J., Simoni, Y., Furio, L., Beaudoin, L., Agerberth, B., Barrat, F., and Lehuen, A. (2013). Crosstalk between neutrophils, B-1a cells and plasmacytoid dendritic cells initiates autoimmune diabetes. Nat Med *19*, 65-73.

Edgar, R.C. (2010). Search and clustering orders of magnitude faster than BLAST. Bioinformatics *26*, 2460-2461.

Endesfelder, D., Engel, M., Davis-Richardson, A.G., Ardissone, A.N., Achenbach, P., Hummel, S., Winkler, C., Atkinson, M., Schatz, D., Triplett, E., *et al.* (2016). Towards a functional hypothesis relating anti-islet cell autoimmunity to the dietary impact on microbial communities and butyrate production. Microbiome *4*, 17.

Fillatreau, S., Sweenie, C.H., McGeachy, M.J., Gray, D., and Anderton, S.M. (2002). B cells regulate autoimmunity by provision of IL-10. Nat Immunol *3*, 944-950.

Frasca, L., and Lande, R. (2012). Role of defensins and cathelicidin LL37 in auto-immune and auto-inflammatory diseases. Curr Pharm Biotechnol *13*, 1882-1897.

Funderburg, N., Lederman, M.M., Feng, Z., Drage, M.G., Jadlowsky, J., Harding, C.V., Weinberg, A., and Sieg, S.F. (2007). Human -defensin-3 activates professional antigen-presenting cells via Toll-like receptors 1 and 2. Proc Natl Acad Sci U S A *104*, 18631-18635.

Ganz, T. (2003). Defensins: antimicrobial peptides of innate immunity. Nat Rev Immunol *3*, 710-720.

Giongo, A., Gano, K.A., Crabb, D.B., Mukherjee, N., Novelo, L.L., Casella, G., Drew, J.C., Ilonen, J., Knip, M., Hyoty, H., *et al.* (2011). Toward defining the autoimmune microbiome for type 1 diabetes. The ISME journal *5*, 82-91.

Gupta, S., and Kaplan, M.J. (2016). The role of neutrophils and NETosis in autoimmune and renal diseases. Nature reviews. Nephrology *12*, 402-413.

Hall, J.C., and Rosen, A. (2010). Type I interferons: crucial participants in disease amplification in autoimmunity. Nat Rev Rheumatol *6*, 40-49.

Hancock, R.E., Haney, E.F., and Gill, E.E. (2016). The immunology of host defence peptides: beyond antimicrobial activity. Nat Rev Immunol *16*, 321-334.

Hasnain, S.Z., Borg, D.J., Harcourt, B.E., Tong, H., Sheng, Y.H., Ng, C.P., Das, I., Wang, R., Chen, A.C., Loudovaris, T., *et al.* (2014). Glycemic control in diabetes is restored by therapeutic manipulation of cytokines that regulate beta cell stress. Nat Med *20*, 1417-1426.

Hill, T., Krougly, O., Nikoopour, E., Bellemore, S., Lee-Chan, E., Fouser, L.A., Hill, D.J., and Singh, B. (2013). The involvement of interleukin-22 in the expression of pancreatic beta cell regenerative Reg genes. Cell Regen (Lond) *2*, 2.

Honda, K., and Littman, D.R. (2016). The microbiota in adaptive immune homeostasis and disease. Nature *535*, 75-84.

Ishigame, H., Zenewicz, L.A., Sanjabi, S., Licona-Limon, P., Nakayama, M., Leonard, W.J., and Flavell, R.A. (2013). Excessive Th1 responses due to the absence of TGF-beta signaling cause autoimmune diabetes and dysregulated Treg cell homeostasis. Proc Natl Acad Sci U S A *110*, 6961-6966.

Kahlenberg, J.M., and Kaplan, M.J. (2013). Little peptide, big effects: the role of LL-37 in inflammation and autoimmune disease. J Immunol *191*, 4895-4901.

Kerkvliet, N.I., Steppan, L.B., Vorachek, W., Oda, S., Farrer, D., Wong, C.P., Pham, D., and Mourich, D.V. (2009). Activation of aryl hydrocarbon receptor by TCDD prevents diabetes in NOD mice and increases Foxp3+ T cells in pancreatic lymph nodes. Immunotherapy *1*, 539-547.

Kinnebrew, M.A., Buffie, C.G., Diehl, G.E., Zenewicz, L.A., Leiner, I., Hohl, T.M., Flavell, R.A., Littman, D.R., and Pamer, E.G. (2012). Interleukin 23 production by intestinal CD103(+)CD11b(+) dendritic cells in response to bacterial flagellin enhances mucosal innate immune defense. Immunity *36*, 276-287.

Klose, C.S., and Artis, D. (2016). Innate lymphoid cells as regulators of immunity, inflammation and tissue homeostasis. Nat Immunol *17*, 765-774.

Lamas, B., Richard, M.L., Leducq, V., Pham, H.P., Michel, M.L., Da Costa, G., Bridonneau, C., Jegou, S., Hoffmann, T.W., Natividad, J.M., *et al.* (2016). CARD9 impacts colitis by altering gut microbiota metabolism of tryptophan into aryl hydrocarbon receptor ligands. Nat Med *22*, 598-605.

Lehrer, R.I. (2004). Primate defensins. Nat Rev Microbiol *2*, 727-738.

Liang, S.C., Tan, X.Y., Luxenberg, D.P., Karim, R., Dunussi-Joannopoulos, K., Collins, M., and Fouser, L.A. (2006). Interleukin (IL)-22 and IL-17 are coexpressed by Th17 cells and cooperatively enhance expression of antimicrobial peptides. J Exp Med *203*, 2271-2279.

Lindroos, J., Svensson, L., Norsgaard, H., Lovato, P., Moller, K., Hagedorn, P.H., Olsen, G.M., and Labuda, T. (2011). IL-23-mediated epidermal hyperplasia is dependent on IL-6. J Invest Dermatol *131*, 1110-1118.

Lund, M.E., Greer, J., Dixit, A., Alvarado, R., McCauley-Winter, P., To, J., Tanaka, A., Hutchinson, A.T., Robinson, M.W., Simpson, A.M., *et al.* (2016). A parasite-derived 68-mer peptide ameliorates autoimmune disease in murine models of Type 1 diabetes and multiple sclerosis. Scientific reports *6*, 37789.

Mansour, S.C., Pena, O.M., and Hancock, R.E. (2014). Host defense peptides: front-line immunomodulators. Trends Immunol *35*, 443-450.

Mantovani, A., Sica, A., and Locati, M. (2007). New vistas on macrophage differentiation and activation. Eur J Immunol *37*, 14-16.

Marino, E., Richards, J.L., McLeod, K.H., Stanley, D., Yap, Y.A., Knight, J., McKenzie, C., Kranich, J., Oliveira, A.C., Rossello, F.J., *et al.* (2017). Gut microbial metabolites limit the frequency of autoimmune T cells and protect against type 1 diabetes. Nat Immunol *18*, 552-562.

Martin, J.C., Beriou, G., Heslan, M., Chauvin, C., Utriainen, L., Aumeunier, A., Scott, C.L., Mowat, A., Cerovic, V., Houston, S.A., *et al.* (2014). Interleukin-22 binding protein (IL-22BP) is constitutively expressed by a subset of conventional dendritic cells and is strongly induced by retinoic acid. Mucosal Immunol *7*, 101-113.

Mauri, C., and Menon, M. (2015). The expanding family of regulatory B cells. Int Immunol *27*, 479-486.

McDonald, D., Price, M.N., Goodrich, J., Nawrocki, E.P., DeSantis, T.Z., Probst, A., Andersen, G.L., Knight, R., and Hugenholtz, P. (2012). An improved Greengenes taxonomy with explicit ranks for ecological and evolutionary analyses of bacteria and archaea. The ISME journal *6*, 610-618.

Melo-Gonzalez, F., and Hepworth, M.R. (2017). Functional and phenotypic heterogeneity of group 3 innate lymphoid cells. Immunology *150*, 265-275.

Mueller, R., Krahl, T., and Sarvetnick, N. (1996). Pancreatic expression of interleukin-4 abrogates insulitis and autoimmune diabetes in nonobese diabetic (NOD) mice. J Exp Med *184*, 1093-1099.

Mulcahy, M.E., Leech, J.M., Renauld, J.C., Mills, K.H., and McLoughlin, R.M. (2016). Interleukin-22 regulates antimicrobial peptide expression and keratinocyte differentiation to control Staphylococcus aureus colonization of the nasal mucosa. Mucosal Immunol *9*, 1429-1441.

Navid, F., Boniotto, M., Walker, C., Ahrens, K., Proksch, E., Sparwasser, T., Muller, W., Schwarz, T., and Schwarz, A. (2012). Induction of regulatory T cells by a murine beta-defensin. J Immunol *188*, 735-743.

Okey, A.B., Franc, M.A., Moffat, I.D., Tijet, N., Boutros, P.C., Korkalainen, M., Tuomisto, J., and Pohjanvirta, R. (2005). Toxicological implications of polymorphisms in receptors for xenobiotic chemicals: the case of the aryl hydrocarbon receptor. Toxicol Appl Pharmacol *207*, 43-51.

Ostaff, M.J., Stange, E.F., and Wehkamp, J. (2013). Antimicrobial peptides and gut microbiota in homeostasis and pathology. EMBO Mol Med *5*, 1465-1483.

Pieterse, B., Felzel, E., Winter, R., van der Burg, B., and Brouwer, A. (2013). PAH-CALUX, an optimized bioassay for AhR-mediated hazard identification of polycyclic aromatic hydrocarbons (PAHs) as individual compounds and in complex mixtures. Environ Sci Technol *47*, 11651-11659.

Pinegin, B., Vorobjeva, N., and Pinegin, V. (2015). Neutrophil extracellular traps and their role in the development of chronic inflammation and autoimmunity. Autoimmun Rev *14*, 633-640.

Qiu, J., Heller, J.J., Guo, X., Chen, Z.M., Fish, K., Fu, Y.X., and Zhou, L. (2012). The aryl hydrocarbon receptor regulates gut immunity through modulation of innate lymphoid cells. Immunity *36*, 92-104.

Riviere, A., Selak, M., Lantin, D., Leroy, F., and De Vuyst, L. (2016). Bifidobacteria and Butyrate-Producing Colon Bacteria: Importance and Strategies for Their Stimulation in the Human Gut. Frontiers in microbiology *7*, 979.

Roohi, A., Tabrizi, M., Abbasi, F., Ataie-Jafari, A., Nikbin, B., Larijani, B., Qorbani, M., Meysamie, A., Asgarian-Omran, H., Nikmanesh, B., *et al.* (2014). Serum IL-17, IL-23, and TGF-beta levels in type 1 and type 2 diabetic patients and age-matched healthy controls. BioMed research international *2014*, 718946.

Rooks, M.G., and Garrett, W.S. (2016). Gut microbiota, metabolites and host immunity. Nat Rev Immunol *16*, 341-352.

Rosser, E.C., and Mauri, C. (2015). Regulatory B cells: origin, phenotype, and function. Immunity *42*, 607-612.

Sabat, R., Ouyang, W., and Wolk, K. (2014). Therapeutic opportunities of the IL-22-IL-22R1 system. Nat Rev Drug Discov *13*, 21-38.

Semple, F., and Dorin, J.R. (2012). beta-Defensins: multifunctional modulators of infection, inflammation and more? J Innate Immun *4*, 337-348.

Semple, F., MacPherson, H., Webb, S., Cox, S.L., Mallin, L.J., Tyrrell, C., Grimes, G.R., Semple, C.A., Nix, M.A., Millhauser, G.L., and Dorin, J.R. (2011). Human beta-defensin 3 affects the activity of pro-inflammatory pathways associated with MyD88 and TRIF. Eur J Immunol *41*, 3291-3300.

Semple, F., Webb, S., Li, H.N., Patel, H.B., Perretti, M., Jackson, I.J., Gray, M., Davidson, D.J., and Dorin, J.R. (2010). Human beta-defensin 3 has immunosuppressive activity in vitro and in vivo. Eur J Immunol *40*, 1073-1078.

Shikhagaie, M.M., Germar, K., Bal, S.M., Ros, X.R., and Spits, H. (2017). Innate lymphoid cells in autoimmunity: emerging regulators in rheumatic diseases. Nat Rev Rheumatol *13*, 164-173.

Shioya, M., Andoh, A., Kakinoki, S., Nishida, A., and Fujiyama, Y. (2008). Interleukin 22 receptor 1 expression in pancreas islets. Pancreas *36*, 197-199.

Simonian, P.L., Wehrmann, F., Roark, C.L., Born, W.K., O'Brien, R.L., and Fontenot, A.P. (2010). gammadelta T cells protect against lung fibrosis via IL-22. J Exp Med *207*, 2239-2253.

Sonnenberg, G.F., Monticelli, L.A., Alenghat, T., Fung, T.C., Hutnick, N.A., Kunisawa, J., Shibata, N., Grunberg, S., Sinha, R., Zahm, A.M., *et al.* (2012). Innate lymphoid cells promote anatomical containment of lymphoid-resident commensal bacteria. Science *336*, 1321-1325.

Sun, J., Furio, L., Mecheri, R., van der Does, A.M., Lundeberg, E., Saveanu, L., Chen, Y., van Endert, P., Agerberth, B., and Diana, J. (2015). Pancreatic beta-Cells Limit Autoimmune Diabetes via an Immunoregulatory Antimicrobial Peptide Expressed under the Influence of the Gut Microbiota. Immunity *43*, 304-317.

Tang, Q., and Bluestone, J.A. (2008). The Foxp3+ regulatory T cell: a jack of all trades, master of regulation. Nat Immunol *9*, 239-244.

Tilg, H., and Adolph, T.E. (2017). Beyond Digestion: The Pancreas Shapes Intestinal Microbiota and Immunity. Cell Metab *25*, 495-496.

Wang, G. (2012). Post-translational Modifications of Natural Antimicrobial Peptides and Strategies for Peptide Engineering. Current biotechnology *1*, 72-79.

Wang, X., Ota, N., Manzanillo, P., Kates, L., Zavala-Solorio, J., Eidenschenk, C., Zhang, J., Lesch, J., Lee, W.P., Ross, J., *et al.* (2014). Interleukin-22 alleviates metabolic disorders and restores mucosal immunity in diabetes. Nature *514*, 237-241.

Wolk, K., Kunz, S., Witte, E., Friedrich, M., Asadullah, K., and Sabat, R. (2004). IL-22 increases the innate immunity of tissues. Immunity *21*, 241-254.

Wolk, K., Witte, E., Wallace, E., Docke, W.D., Kunz, S., Asadullah, K., Volk, H.D., Sterry, W., and Sabat, R. (2006). IL-22 regulates the expression of genes responsible for antimicrobial defense, cellular differentiation, and mobility in keratinocytes: a potential role in psoriasis. Eur J Immunol *36*, 1309-1323.

Xiu, Y., Wong, C.P., Bouaziz, J.D., Hamaguchi, Y., Wang, Y., Pop, S.M., Tisch, R.M., and Tedder, T.F. (2008). B lymphocyte depletion by CD20 monoclonal antibody prevents diabetes in nonobese diabetic mice despite isotype-specific differences in Fc gamma R effector functions. J Immunol *180*, 2863-2875.

Xue, J., Nguyen, D.T., and Habtezion, A. (2012). Aryl hydrocarbon receptor regulates pancreatic IL-22 production and protects mice from acute pancreatitis. Gastroenterology *143*, 1670-1680.

Yang, M., Charlton, B., and Gautam, A.M. (1997). Development of insulitis and diabetes in B cell-deficient NOD mice. J Autoimmun *10*, 257-260.

Zanvit, P., Konkel, J.E., Jiao, X., Kasagi, S., Zhang, D., Wu, R., Chia, C., Ajami, N.J., Smith, D.P., Petrosino, J.F., *et al.* (2015). Antibiotics in neonatal life increase murine susceptibility to experimental psoriasis. Nature communications *6*, 8424.

Zasloff, M. (2002). Antimicrobial peptides of multicellular organisms. Nature *415*, 389-395.

Zhang, L.J., and Gallo, R.L. (2016). Antimicrobial peptides. Curr Biol *26*, R14-19.

Zhao, B., Bohonowych, J.E., Timme-Laragy, A., Jung, D., Affatato, A.A., Rice, R.H., Di Giulio, R.T., and Denison, M.S. (2013). Common commercial and consumer products contain activators of the aryl hydrocarbon (dioxin) receptor. PLoS One *8*, e56860.

Zheng, Y., Valdez, P.A., Danilenko, D.M., Hu, Y., Sa, S.M., Gong, Q., Abbas, A.R., Modrusan, Z., Ghilardi, N., de Sauvage, F.J., and Ouyang, W. (2008). Interleukin-22 mediates early host defense against attaching and effacing bacterial pathogens. Nat Med *14*, 282-289.

Zhou, L. (2016). AHR Function in Lymphocytes: Emerging Concepts. Trends Immunol *37*, 17-31.

Figure legends

Figure 1 MBD14 is expressed by pancreatic endocrine cells and is protective against autoimmune diabetes. (**A, B**) Islets from female mice (**A**) or from female healthy subject (**B**) were stained for insulin (green), mBD14 (**A**) or hBD3 (**B**) (red), glucagon (blue) and DNA (grey). Data are representative of 6 independent experiments. (**C, D**) mRNA expression of mBD14 was analyzed by RT-qPCR in islets from female or male mice. Data are the median +/− interquartile range of 12 to 15 independent mice per group. (**E**) IFNγ expression by $OVA_{257-264}$-reactive (negative control) or $IGRP_{206-214}$-reactive $CD8^+$ T cells were determined in islets from NOD mice treated with mBD14, scmBD14, or vehicle (d−10). Data are the frequency of $IFN\gamma^+$ cells among T cell population and are representative or the median +/− interquartile range of 6 to 9 independent mice per group. (**F**) Female NOD mice were treated with mBD14, scmBD14, or vehicle and incidence of diabetes was followed, n=12 mice per group. (**G**) Immune cell populations in islets from female NOD mice treated with mBD14 or vehicle (d–3) were determined by flow cytometry. Data are the frequency of gated cells ($CD19^+$ B cell, $TCR\beta^+$ T cell, $F4/80^-$ $CD11c^+$ DC and $F4/80^+$ $CD11b^+$ macrophage) among the $CD45^+$ population (left panel) and the number of cells per mouse (right panel). Data are representative and are the median +/− interquartile range of 9 independent mice per group. See also Figure S1 and S2.

Figure 2 MBD14 induces pancreatic regulatory B cells *via* TLR2. (**A, B** and **D, E**) NOD mice were treated with mBD14 or vehicle (d−3). B cells ($CD19^+$ $CD11b^-$) from islets, lymph nodes and spleen were analyzed by flow cytometry. Results show the frequency of positive cells and the MFI of indicated marker among B cell population. Data are representative and are the median +/− interquartile range of 6–9 independent mice per group. (**C**) Incidence of diabetes of NOD mice treated with mBD14 and anti-IL4 neutralizing mAb. (**F, G**) Pancreatic B cells

from NOD mice were cultured for 4 days in presence of growing dose (µg.ml^{-1}) of mBD14 or vehicle. Results show the frequency of positive cells and the MFI of indicated marker among B cells. Data are representative and are the median +/− interquartile range of 5 independent experiments with 4 mice pooled as source of B cells in each experiment. See also Figure S2.

Figure 3 MBD14 induces pancreatic regulatory macrophages and Treg cells. (**A**) Macrophage sub-populations in islets from NOD mice treated with mBD14 or vehicle (d–5) and treated with anti-IL4 or anti-CD20 mAbs. Data show the frequency of gated cells among macrophages (F4/80$^+$ CD11b$^+$) and the ratio between the frequency of inflammatory (M1, CD11c$^+$ CD206$^-$) and regulatory (M2, CD11c$^-$ CD206$^+$) macrophages. Data are representative and are the median +/− interquartile range of 9 independent mice per group. (**B**) Cytokine intracellular expression in pancreatic macrophages. Results show the MFI of indicated marker among macrophages. Data are representative and are the median +/− interquartile range of 6 to 9 independent mice per group. (**C,D**) Regulatory T cells were analyzed in islets from NOD mice treated with mBD14 or vehicle (day−10). In **D**, mice were treated with anti-IL4 or anti-TGFβ neutralizing mAbs. Results show the frequency of Treg cells (Foxp3$^+$) among the CD4$^+$ T cell population. Data are representative and are the median +/– interquartile range of 6 to 9 independent mice per group. (**E**) Pancreatic myeloid cells (CD11b$^+$) or B cells (CD19$^+$) were isolated from NOD mice treated with mBD14 (^{14}) or vehicle (^{0}) (day−4) and cultured with naïve BDC2.5 T cells. Data show the frequency and number (in brackets) of Treg cells (Foxp3$^+$ CD25$^+$) among the CD4 T cell population. Data are the median +/− interquartile range of 5 independent experiments with 4 mice pooled per group in each experiment. See also Figure S3.

Figure 4 IL-22 stimulates pancreatic mBD14 expression and is produced by pancreatic innate lymphoid cells. (**A**) mRNA expression of IL22 was analyzed by RT-qPCR in islets. (**B**) mRNA

expression of mBD14 in NOD mice treated with rmIL-22Fc or vehicle (h−3). (**C**) mBD14 mRNA expression in isolated islets cultured in presence of rmIL-22 (h−3). (**D**) Human islets were cultured and analyzed as in (**C**). (**E**) Innate lymphoid cells (ILCs) were analyzed in islets. Data show the frequency and number of ILCs ($CD127^+$ $CD90^+$ Lin^-) among $CD45^+$ population. (**F**) The subtype of ILCs were analyzed in islets according to their expression of transcription factors. Data show the frequency of ILC3s ($RoR\gamma t^+$ $GATA3^-$) among the pancreatic ILC population. Data are representative and are the median +/− interquartile range of 6 independent mice per group. (**G**) Data show the frequency and number of $IL\text{-}22^+$ cells among the pancreatic ILCs after stimulation with rmIL-23 plus PMA/ionomycin. Data are representative and are the median +/− interquartile range of 7 independent mice per group. (**H**) C57BL/6 islets were stained for insulin (green), CD5 (red), IL-22 (blue) and DNA (grey). Data are representative of 5 independent experiments. See also Figure S4-6.

Figure 5 Gut microbiota controls pancreatic mBD14 expression. (**A-C**) Six-weeks-old BALB/c mice were treated for 10 days with antibiotic cocktail (ABX). Seven days later, IL-22 concentration in the serum was determined by ELISA (**A**) and mRNA expression of IL22 and mBD14 in the islets were determined by RT-qPCR (**B, C**). Data are the median +/− interquartile range of 9 independent mice per group. (**D**) Six-weeks-old NOD mice were transferred with gut microbiota from the different mouse strains (→). Seven days later mRNA expression of mBD14 in islets were determined by RT-qPCR. Data are the median +/− interquartile range of 6 independent mice per group. (**E-G**) Gut microbiota is altered in NOD mice. Gut microbiota composition was determined by 16S rDNA sequencing in the feces. Differential analysis (LEFSE) between mouse strains at the phylum level (**E**) and family level (**F**) is shown. See also Figure S7.

Figure 6 AHR ligands stimulates pancreatic mBD14 expression. (**A, B**) Expression of Cyp1a1 and IL22 mRNA were analyzed in islets from BALB/c mice treated with FICZ or vehicle for indicated time points. (**C**) Expression of mBD14 mRNA was analyzed in islets from BALB/c mice treated with FICZ, Indole or vehicle for 12h. Data are the median +/− interquartile of 5 independent mice per group. (**D-F**) Expression of Cyp1a1, IL22 and mBD14 mRNA were determined in BALB/c islets cultured for 48 h with FICZ and anti-IL-22 neutralizing mAb. Data are the median +/− interquartile of 5 to 6 independent mice per group. (**G**) Min6 β-cells were treated with increasing doses of FICZ or IL-22 (200 $ng.ml^{-1}$) for 24 h. The expression of mBD14 mRNA was determined by RT-qPCR. Data are the median +/− interquartile of 5 independent experiments. (**H, I**) AHR ligand activity was determined in the serum (**H**) and feces (**I**) using reporter bioassay. Data are the median +/− interquartile of 5 to 9 independent mice per group. (**J**) mRNA expression of Cyp1a1 and mBD14 were determined in islets cultured for 48 h with growing dose ($ng.ml^{-1}$) of FICZ. Data are the median +/− interquartile of 4 to 5 independent experiments with 4 mice pooled per group per experiment. See also Figure S7.

Figure 7 Butyrate induces IL-23 expression in the pancreas stimulating mBD14 expression. (**A**) IL23 mRNA expression was determined in islets. (**B**) Expression of IL-23 in pancreatic myeloid cells ($CD11b^{+}$ $CD19^{-}$) was determined by flow cytometry. Results show the frequency of $IL\text{-}23^{+}$ cells and the MFI of IL-23 among myeloid cells. Data are representative and are the median +/− interquartile range of 6 independent mice per group. (**C-E**) mRNA expression of IL22 and mBD14 were determined in islets from BALB/c mice treated with rmIL-23 (h−2) and the level of IL-22 was analyzed in the serum. Data are the median +/− interquartile range of 6 to 7 independent mice per group. (**F-I**) Expression of IL23, IL22 and mBD14 mRNA were determined in islets from BALB/c mice treated with butyrate daily for 5 days. The level of IL-

23 was determined in the serum. Data are the median +/− interquartile of 6 independent mice per group. (**J**-**L**) Expression of IL23, IL22 and mBD14 mRNA was determined in BALB/c islets cultured for 18 h with butyrate and anti-IL-22 neutralizing mAb. Data are the median +/− interquartile of 5 to 7 independent mice per group. (**M**) IL-23 expression by pancreatic myeloid cells was determined by flow cytometry in BALB/c mice treated with butyrate. Results show the frequency of IL-23^{+} cells and the MFI of IL-23 among myeloid cells. Data are the median +/− interquartile of 6 independent mice per group. See also Figure S7.

STAR METHODS

KEY RESOURCES TABLE

Reagent or Resource	Source	Identifier
Antibodies		
CD16/CD32	Biolegend	Cat# 101301, RRID:AB_312800
CD45	Biolegend	Cat# 103149, RRID:AB_2564590
CD11b	Biolegend	Cat# 101237, RRID:AB_11126744
F4/80	Biolegend	Cat# 123113, RRID:AB_893490
CD11c	Biolegend	Cat# 117349, RRID:AB_2563905
TCRβ	Biolegend	Cat# 109234, RRID:AB_2562350
TCRγ/δ	Biolegend	Cat# 107512, RRID:AB_492900
CD19	Biolegend	Cat# 115549, RRID:AB_2563066
CD206	Biolegend	Cat# 141705, RRID:AB_10896421
CD5	Miltenyi	Cat# 130-102-574, RRID:AB_2658608
CD1d	Biolegend	Cat# 140805, RRID:AB_10643277
CD21	Biolegend	Cat# 123412, RRID:AB_2085160
CD24	Biolegend	Cat# 138503, RRID:AB_10576359
CD138	Biolegend	Cat# 142515, RRID:AB_2562336
B220	Biolegend	Cat# 103209, RRID:AB_312994
TLR2	Biolegend	Cat# 148603, RRID:AB_2564119
CD127	Biolegend	Cat# 135024, RRID:AB_11218800
LAP	Biolegend	Cat# 141409, RRID:AB_2561591
TNFα	Thermo Fisher Scientific	Cat# 51-7321-82, RRID:AB_469813
IL-12	Thermo Fisher Scientific	Cat# 12-7123-41, RRID:AB_1963609
IL-4	Thermo Fisher Scientific	Cat# 12-7041-71, RRID:AB_466154
IL-10	Thermo Fisher Scientific	Cat# 51-7101-80, RRID:AB_469802
IL-23	Thermo Fisher Scientific	Cat# 50-7023-80, Clone fc23-cpg
IDO	Biolegend	Cat# 654003, RRID:AB_2564584
IL-22	Biolegend	Cat# 516404, RRID:AB_2124255
CD4	BD	Cat# 561025, RRID:AB_2034006
CD8α	BD	Cat# 553036, RRID:AB_394573
IFNγ	Thermo Fisher Scientific	Cat# 51-7311-82, RRID:AB_469809
Foxp3	Thermo Fisher Scientific	Cat# 51-5773-80, RRID:AB_469793
RoRγt	Thermo Fisher Scientific	Cat# 17-6981-80, RRID:AB_2573253
GATA3	Biolegend	Cat# 653812, RRID:AB_2563219
Ki67	Thermo Fisher Scientific	Cat# 50-5698-80, RRID:AB_2574234
Insulin	Abcam	Cat# ab7842, RRID:AB_306130
Glucagon	Abcam	Cat# ab10988, RRID:AB_297642
CD5	Biolegend	Cat# 100602, RRID:AB_312731
mBD14	Mybiosource	#MBS1490249
hBD3	Abcam	Cat# ab19270, RRID:AB_444821
TLR2	Biolegend	Cat# 309710, RRID:AB_2204581
CD90.2	Thermo Fisher Scientific	Cat# 17-5321-81, RRID:AB_469454
Goat IgG Isotype	Biolegend	Clone poly24030
Goat anti-guinea pig	Thermo Fisher Scientific	Cat# A-11073, RRID:AB_142018

Goat anti-mouse	Thermo Fisher Scientific	Cat# A32728, RRID:AB_2633277
Goat anti-rabbit	Thermo Fisher Scientific	Cat# A32732, RRID:AB_2633281
Donkey anti-guinea pig	Jackson Immunoresearch	Cat# 706-545-148, RRID:AB_2340472
Donkey anti-rat	Abcam	ab150150
Donkey anti-goat	Thermo Fisher Scientific	Cat# A-21084, RRID:AB_2535741
Peptides		
mBD14	Mybiosource	FLPKTLRKFFCRIRGGRCAVLNCLGKEEQIGRCSNSGRKCCRKKK
Scrambled mBD14	Proteogenix	LILRFCFLGTGCRGNKLKVRPARFCSRKEKKGKRSQINRCCKEGC
Blocking/Neutralizing molecules		
αIL-4 mAb	BioXcell	Cat# BE0045, RRID:AB_1107707
αTGFβ mAb	BioXcell	Cat# BE0057, RRID:AB_1107757
αCD20 mAb	BioXcell	Cat# BE0302, RRID:AB_2715460
αIL-22 mAb	Thermo Fisher Scientific	Cat# 16-7222-85, RRID:AB_2016574
αTLR2 mAb	Invivogen	Cat# mab-htlr2, RRID:AB_763707
CU-CTP22	Tocris	#4884/10
Recombinant molecules		
rmIL-22	Biolegend	#576208
rmIL-23	Biolegend	#589008
rmIL-22-Fc	Adipogen	#CHI-MF-12022-C050
rmGM-CSF	R&D	#415-ML-050
rmM-CSF	R&D	#416-ML-050
Biochemicals		
6-Formylindolo-[3,2-b]-carbazole	Tocris	#5304
Indole-3-carboxaldehyde	Sigma-Aldrich	#129445
Sodium butyrate	Sigma-Aldrich	#B5887
Lipopolysaccharides	Sigma-Aldrich	#L6529
L-Cysteine hydrochloride	Sigma-Aldrich	#30120
Antibiotics		
Metronidazole	Sigma-Aldrich	#M3761
Vancomycin	Sigma-Aldrich	#V2002
Neomycin	Sigma-Aldrich	#N1142
Gentamicin	Sigma-Aldrich	#G1397
Ampicillin	Sigma-Aldrich	#A9518
Amphotericin B	Sigma-Aldrich	#A9528
Streptomycin	Sigma-Aldrich	#S6501
Specific reagents for islet isolation		
Collagenase P	Sigma-Aldrich	#COLLP-RO ROCHE
Ficoll® PM400	Sigma-Aldrich	#F4375
Non-enzymatic cell dissociation solution	Sigma-Aldrich	#C5789
DNAse 1	Sigma-Aldrich	#DN-25
Commercial Assays		
Nucleospin RNA XS kit	Macherey-Nagel	#740902.250
High capacity cDNA reverse transcription kit	ThermoFisher	#4368814

Takyon ROX SYBR MasterMix blue dTTP	Eurogentec	#UF-RSMT-B0710
RNeasy Kit	Qiagen	#74106
IL-22 ELISA kit	Biolegend	#436304
IL-23 ELISA kit	Biolegend	#433707
Anti-biotin microbeads	Miltenyi	#130-097-046
Naive $CD4^+$ T cell isolation kit	Miltenyi	#130-104-453
Foxp3 staining kit	eBioscience	#00-5523-00
True-Nuclear™ Transcription Factor kit	Biolegend	#424401
Glukotest kit	Roche	Accu-Chek® Performa
Oligonucleotides		
mGAPDH FW	Eurofins	5'-CCGTAGACAAAATGGTGAAGG-3'
mGAPDH REV	Eurofins	5'-CGTGAGTGGAGTCATACTGGA-3'
mBD14 FW	Eurofins	5'-GTATTCCTCATCTTGTTCTTGG-3'
mBD14 REV	Eurofins	5'-AAGTACAGCACACCGGCCAC-3'
IL22 FW	Eurofins	5'-CATGCAGGAGGTGGTACCTT-3'
IL22 REV	Eurofins	5'-CAGACGCAAGCATTTCTCAG-3'
IL23 FW	Eurofins	5'-TGGTTGTGACCCACAAGGAC-3'
IL23 REV	Eurofins	5'-AGGGAGGTGTGAAGTTGCTC-3'
hBD3 FW	Eurofins	5'-CTTCTGTTTGCTTTGCTCTTCC-3'
hBD3 REV	Eurofins	5'-CACTTGCCGATCTGTTCCTC-3'
Cyp1a1 FW	Eurofins	5'-CAGGATGTGTCTGGTTACTTTGAC-3'
Cyp1a1 REV	Eurofins	5'-CTGGGCTACACAAGACTCTGTCTC-3'
Reg3g FW	Eurofins	5'-TTCCTGTCCTCCATGATCAAAA-3'
Reg3g REV	Eurofins	5'-CATCCACCTCTGTTGGGTTCA-3'
CCL3 FW	Eurofins	5'-CCTGCTGCTTCTCCTACAGC-3'
CCL3 REV	Eurofins	5'-CTGCCTCCAAGACTCTCAGG-3'
CCL5 FW	Eurofins	5'-CCCTCACCATCATCCTCACT-3'
CCL5 REV	Eurofins	5'-CCTTCGAGTGACAAACACGA-3'
CXCL9 FW	Eurofins	5'-CTGGGCAGAAGTTCCGTCTT-3'
CXCL9 REV	Eurofins	5'-TTACCGAAGGGAGGTGGACA-3'
CXCL10 FW	Eurofins	5'-GTCTGAGTCCTCGCTCAAGT-3'
CXCL10 REV	Eurofins	5'-TCGCACCTCCACATAGCTTAC-3'
CXCL13 FW	Eurofins	5'-GAATGCTCAAGCTCCGTTGC-3'
CXCL13 REV	Eurofins	5'-TGGGTTGTCACTAAATGCCTGT-3'
Mouse		
NOD mice	Internal breeding	JAX: #001976
NOD *rag*$^{-/-}$	Internal breeding	MGI:97848
NOD *myd88*$^{-/-}$	Internal breeding	MGI:108005
C57BL/6J	Internal breeding	JAX: #000664
C57BL/6J *rag*$^{-/-}$	Internal breeding	JAX: #008309
C57BL/6J *IL22*$^{-/-}$	UMR7355, France	
BALB/cJ	Internal breeding	JAX: #000651
Cells		
Human islets	Tebu-bio/Prodo laboratories	#HIR-IEQ
Min 6 cells	ATCC	#CRL-11506™
Software		
Graphpad Prism v.6		https://www.graphpad.com/
FlowJo v. 10		https://www.flowjo.com/
Icy		http://icy.bioimageanalysis.org/

CONTACT FOR REAGENT AND RESOURCE SHARING

Further information and requests for resources and reagents should be directed to and will be fulfilled by the Lead Contact, J. Diana (julien.diana@inserm.fr).

EXPERIMENTAL MODEL DETAILS

Mice and treatments

Female BALB/c, C57BL/6J, NOD, NOD *rag*$^{-/-}$, C57BL/6J *rag*$^{-/-}$, C57BL/6J *IL22*$^{-/-}$ and NOD *myd88*$^{-/-}$ mice between 10 and 12 weeks of age were used, bred and housed in specific pathogen-free conditions. In some experiments, male mice were used as indicated in the figure. Recombinant mBD14 (Mybiosource) (FLPKTLRKFFCRIRGGRCAVLNCLGKEEQIGRCSNSGRKCCRKKK), and scrambled (sc) mBD14 (Proteogenix) (LILRFCFLGTGCRGNKLKVRPARFCSRKEKKGKRSQINRCCKEGC) were produced under aseptic conditions and provided after endotoxin removal processing. Peptides were administrated intraperitoneally (i.p.) at the dose of 10 µg diluted in 200 µl of vehicle (PBS-1% H2O). For in vivo blocking experiments, mice were treated (200 µg per i.p. injection at day −1, 1 and 3 post mBD14 treatment) with anti-IL4 (11B11) or anti-TGFβ (1D11) mAbs (BioXcell) or relevant isotype controls. For in vivo depleting experiments, mice were treated (200 µg per i.p. injection at day 0 and 1 post mBD14 treatment) with anti-CD20 (SA271G2) mAb (Biolegend) or relevant isotype controls. In some experiments, mice were i.p. injected with: rmIL-22Fc (Adipogen), 200 µg in 200µl PBS for 3 h; rmIL-23 (Biolegend), 2 µg in 200µl PBS for 2 h; 6-Formylindolo-[3,2-b]-carbazole (FICZ, Tocris) 2 µg in 200 µl PBS for indicated time; indole (Sigma-Aldrich) 100 µg in 200 µl PBS for 12 h; sodium butyrate (Sigma-Aldrich) daily for 5 days with 1 mg per day in 200 µl PBS. For antibiotic treatment, mice were given 1 g.l^{-1} metronidazole (Sigma-Aldrich), 0.5 g.l^{-1} vancomycin (Sigma-Aldrich), 1 g.l^{-1} ampicillin

(Sigma-Aldrich), 1 g.l^{-1} gentamicin (Sigma-Aldrich) and 1 g.l^{-1} neomycin (Sigma-Aldrich) by daily oral gavage of 200 µL in antibiotic solution (100% H20). In parallel with the antibiotic treatment, mice were treated per os with 200 mg l^{-1} amphotericin B of 100 µL in solution (100% H20) to avoid occasional overgrowth of Candida spp. For microbiota transfer experiment, the gut microbiota was transferred between groups of mice by initially depleting the native microbiota with a single oral dose of streptomycin (20 mg) 24 h prior the transplantation. Fresh fecal pellets (120 mg) from 5 donor mice were collected and placed in 1 ml of transfer buffer (pre-reduced sterile cold PBS containing 0.05% cysteine HCl (Sigma-Aldrich)). The fecal pellets were homogenized, centrifuged at 800 g for 2 min, and 50 µl fecal supernatant was orally inoculated to recipient mice over the subsequent 15 days for a total of 6 times. All animal experimental protocols were approved by the ethic committee for animal experimentation (APAFIS#3535-2015092416202090).

Spontaneous diabetes incidence

Eight-weeks-old NOD female mice received one injection of mBD14 or scmBD14 (10 µg) per week during two weeks or similar injections of vehicle (PBS-1% H2O). In some conditions, mice were treated (200 µg per injection at day −1, 1, 3, 6 and 9 post mBD14 treatment) with anti-IL4 (11B11) or relevant isotype control. Overt diabetes was defined as two positive urine glucose tests, confirmed by a glycemia >200 mg.dl^{-1}. Glukotest kit was purchased from Roche. Glucose tests and measure of glycemia were performed in a blind fashion.

METHOD DETAILS

Preparation of pancreatic islets

Pancreata were perfused with a solution of collagenase P in HBSS-1% HEPES (0.75 mg.ml^{-1}, Roche), then dissected free from surrounding tissues. Pancreata were digested at 37°C for 8

min. Digestion was stopped by adding HBSS-10% FCS-1% EDTA followed by extensive washes. For flow cytometry analysis, islets were isolated on a discontinuous Ficoll® PM400 gradient (Sigma-Aldrich) and then cells were released from the islets by incubation at 37°C for 6 min in non-enzymatic cell dissociation solution (Sigma-Aldrich). For islets culture, cytology and RT-qPCR, to avoid potential contamination by exocrine tissue, islets were purified by handpicking in 3 consecutive baths of HBSS-10% FCS supplemented with 1% DNAse 1.

RT-qPCR

Total RNA was isolated using the Nucleospin RNA XS kit (Macherey-Nagel) from a minimum of 100 handpicked islets per mouse. RNA was reverse transcribed to synthesized cDNA using the high capacity cDNA reverse transcription kit (ThermoFisher) and measurements were performed by qPCR using Takyon™ ROX SYBR® MasterMix dTTP blue (Eurogentec) on a 7900HT Fast System (Applied Biosystems). Resulting levels of fluorescence were submitted to relative quantification by normalization against a housekeeping gene (GAPDH) and expressed as $2^{-(\Delta CT)}$ values.

Flow cytometry

Single cell suspensions were prepared from various tissues and were stained for 30 min at 4°C after FcγRII/III blocking with anti-CD16/CD32 (Biolegend, 93) monoclonal antibody (mAb). Staining buffer was PBS containing 2% FCS, 0.5% EDTA and 0.1% sodium azide. Surface staining was performed with the following mAbs against: CD45 (eBioscience, 30-F11), CD11b (eBioscience, M1/70), F4/80 (eBioscience, BM8), CD11c (eBioscience, N418), TCRβ (eBioscience, H57-597), TCRγ/δ (eBioscience, UC7-13D5), CD19 (eBioscience, 1D3), CD206 (Biolegend, C068C2), CD5 (Miltenyi, 53-7.3), CD1d (Biolegend, K253), CD21 (Biolegend, 7E9), CD24 (Biolegend, 30-F1), B220 (Biolegend, RA3-6B2), CD138 (Biolegend, 281-2),

TLR2 (Biolegend, CB225), CD127 (Biolegend, A7R34), -CD90.2 (eBioscience, 53-2.1). Lin markers are a mix of anti-CD19, -CD5, -CD3ε , -B220, -CD11b, and -CD11c mAbs. For measurement of active TGFβ, cells were surface stained with anti-LAP mAb (eBioscience, TW7-16B4). For cytokine expression, cell suspensions were incubated 5 h at 37°C with the relevant stimulus, if required, in the presence of a protein transport inhibitor cocktail (eBioscience), surface stained, fixed and then intracellularly stained using the intracellular staining kit (Biolegend). For macrophages and DCs, cell suspension was incubated with LPS (1 $\mu g.ml^{-1}$, Sigma-Aldrich) and stained with anti-TNFα (eBioscience, MP6-XT22), -IL-12 (eBioscience, C17.8), -IL-4 (eBioscience, 11B11), -IL-10 (eBioscience, JES5-16E3) and -IL-23 (eBioscience, fc23-cpg). For innate lymphoid cells, cell suspension was incubated with rmIL-23 (10 ng.ml-1, Miltenyi) plus PMA/ionomycin (both 500 $ng.ml^{-1}$, Sigma-Aldrich) and stained with anti-IL-22 pAb (Biolegend, poly5164) or control isotype (goat IgG, Biolegend, poly24030). For diabetogenic $CD8^+$ T cells, cell suspension was incubated with bone-marrow derived DCs loaded with $IGRP_{206–214}$ peptide and stained with anti-CD8α (BD, 53-6.7) and anti-IFNγ mAbs (eBioscience, XMG1.2). For B cells, cell suspension was incubated without additional stimulus and stained with anti-IL-4 (eBioscience, 11B11), -IL-10 (eBioscience, JES5-16E3) and -IDO (Biolegend, 2E2/IDO1) mAbs. For regulatory T cell detection, cells were surface stained with anti-TCRβ, -CD4 (BD, RM4-5), fixed and then stained for Foxp3 (eBioscience, FJK-16s) expression, using the Foxp3 staining kit (eBioscience). For staining of transcription factors RoRγt, GATA3 (eBioscience, B2D and 16E10A23) and ki67 (eBioscience, SolA15), cells were stained using the True-Nuclear™ Transcription Factor kit (Biolegend). In all experiments dead cells were excluded using Fixable Viability Dye (eBioscience). Stained cells were analyzed on a Becton Dickinson Fortessa flow cytometer. Data were analyzed with Flowjo™ v10 software.

Immunocytology

Handpicked pancreatic islets were seeded on SuperFrost Gold Plus microscope slide. For β-defensin staining, islets were fixed, blocked with goat serum, permeabilized, and stained with anti-insulin pAb (Abcam, ab7842), anti-glucagon mAb (Abcam, ab10988) and anti-mBD14 pAb (Mybiosource, MBS1490249) or anti-hBD3 pAb (Abcam, ab19270), overnight at 4°C. After washing, second-step reagents were applied: anti-guinea pig-AlexaFluor488, anti-mouse-Alexa647 and anti-rabbit-AlexaFluor555 pAbs (Invitrogen). For IL-22 staining, isolated islets were incubated 5 h at 37°C with rIL-23 (10 ng.ml–1, Miltenyi) and PMA/ionomycin (both 500 $ng.ml^{-1}$, Sigma-Aldrich) in the presence of a protein transport inhibitor cocktail. Then islets were fixed, blocked with donkey serum, permeabilized and stained with anti-insulin pAb (Abcam), anti-CD5 mAb (Biolegend, 53-7.3) and anti-IL-22 mAb (Biolegend, poly5164), overnight at 4°C. After washing, second-step reagents were applied: anti-guinea pig-AlexaFluor488, anti-rat-Alexa555 and anti-goat-AlexaFluor647 pAbs (Invitrogen). Nuclei were stained with DAPI. Image acquisition was performed on Necker Institute Imaging Facility using a Leica SP8 confocal microscope.

In vitro B cell culture

B cells were magnetically isolated using MACS cell separation system (anti-biotin beads, Miltenyi). $CD19^+$ B cells ($2x10^5$ cells per well) from pancreatic lymph nodes or pancreatic islets of 10-weeks-old female WT or *myd88*$^{-/-}$ NOD mice were incubated for 4 days in complete IMDM with growing doses (0.1 to 10 $\mu g.ml^{-1}$) of mBD14 or vehicle. Blocking reagents were added as indicated: neutralizing anti-TLR2 mAb (5 $\mu g.ml^{-1}$, Invivogen), TLR1/2 heterodimer antagonist CU-CTP22 (10 µM, Tocris).

In vitro Treg cell induction

All cells were magnetically isolated using MACS cell separation kit and system (Miltenyi). $CD62L^+CD4^+CD25^-$ BDC2.5 T cells ($4x10^4$ cells per well) from splenocytes of BDC2.5 TCR transgenic NOD mice were incubated with $2x10^3$ myeloid cells ($CD11b^+$) and or $2x10^3$ B cells ($CD19^+$) obtained from pancreatic islets of NOD mice treated with mBD14 (10 $\mu g.ml^{-1}$) or vehicle 4 days earlier. Cell culture was performed for 4 days in complete IMDM with 20 $ng.ml^{-1}$ of peptide 1040-51, a mimotope of BDC2.5 T cells.

In vitro pancreatic islet culture

Mouse and human (Tebu-bio) pancreatic islets isolated by handpicking were cultured in complete IMDM (10% FBS, 0.6 $g.l^{-1}$ L-glutamine, 100 $U.ml^{-1}$ penicillin streptomycin, 100 µM 2-mercaptoethanol, 4.5 $g.l^{-1}$ D-Glucose). In some experiments, islets were treated with: rmIL-22 (100 $ng.ml^{-1}$, Biolegend) for 4 h; FICZ (50 $ng.ml^{-1}$, Tocris) for 12 h; rmIL-23 (20 $ng.ml^{-1}$, Miltenyi) for 18 h; sodium butyrate (1 $mg.ml^{-1}$, Sigma-Aldrich) for 48 h with or without neutralizing anti-IL-22 mAb (1 $\mu g.ml^{-1}$, IL22JOP, eBioscience).

Cytokine quantification

The level of IL-23 and IL-22 in the serum was determined using commercial ELISA kit (Biolegend).

RNAseq gene expression profiling

Total RNA were isolated from pancreatic islets (>150) using the RNeasy Kit (QIAGEN) including a DNAse treatment step. RNA quality was assessed using RNA Screen Tape 6000 Pico LabChips with the Tape Station (Agilent Technologies) and RNA concentration was measured by spectrophometry using the Xpose (Trinean). RNAseq libraries were prepared starting from 1 µg of total RNA using the TruSeq Stranded mRNA LT Sample Prep Kit

(Illumina) as recommended by the manufacturer. Half of the oriented cDNA produced from the poly-A^+ fraction was PCR amplified (11 cycles). The RNAseq libraries were sequenced on an Illumina HiSeq2500 (Paired-End sequencing 130x130 bases, High Throughput Mode). A mean of 23 million of paired-end reads was produced per library sample (between 21 to 25 million of passing filter reads). The generated data were analyzed using the Ingenuity Pathway Analysis software (Qiagen).

AHR ligand activity measurement

The BioDetection Systems Company performed experiments to determine AHR ligand activity in the serum using a reporter assay system (PAH-CALUX bioassay) (Pieterse et al., 2013). AHR activity in stool samples was determined in the laboratory using the H1L1.1c2 cell line, containing a stably integrated dioxin-response element (DRE)-driven firefly luciferase reporter plasmid pGudLuc1.1, as described previously (Lamas et al., 2016; Zhao et al., 2013).

Analysis of AHR ligand composition

The concentrations of Indole-3-Lactic acid, Indole-3-aldehyde, Indole-3-Acetic acid in the serum and the caecal content of mice were determined by a specific method using HPLC-coupled to high resolution mass spectrometry. This quantitative method has been validated analytically on both types of samples in order to meet the criteria FDA Guidance for Industry.

16S rDNA gene sequencing

Murine stools were frozen at -80°C immediately after emission and stored until further processing. Then, as previously described (Lamas et al., 2016), feces samples were weighed and then resuspended for 10 min at room temperature in 250 µl of 4 M guanidine thiocyanate in 0.1 M Tris (pH 7.5) (Sigma-Aldrich) and 40 µl of 10% N-lauroyl sarcosine (Sigma-Aldrich).

After the addition of 500 µl of 5% N-lauroyl sarcosine in 0.1 M phosphate buffer (pH 8.0), the 2-ml tubes were incubated at 70 °C for 1 h. One volume (750 ml) of a mixture of 0.1- and 0.6-mm-diameter silica beads (Sigma-Aldrich) (previously sterilized by autoclaving) was added, and the tube was shaken at 6.5 m/s three times for 30 s each in a FastPrep (MP Biomedicals) apparatus. Polyvinylpolypyrrolidone (15 mg) was added to the tube, which was then vortexed and centrifuged for 5 min at 20,000g. After recovery of the supernatant, the pellets were washed with 500 µl of TENP (50 mM Tris (pH 8), 20 mM EDTA (pH 8), 100 mM NaCl, 1% polyvinylpolypyrrolidone) and centrifuged for 5 min at 20,000g, and the new supernatant was added to the first supernatant. The washing step was repeated two times. The pooled supernatant (about 2 ml) was briefly centrifuged to remove particles and then split into two 2-ml tubes. DNA was isolated from the feces of the various mouse strains using the Nucleospin DNA stool (Macherey-Nagel). Microbial diversity was determined for each sample by targeting a portion of the ribosomal genes. A 16S rDNA gene fragment comprising the V3 and V4 hypervariable regions (16S (sense) 5′-TACGGRAGGCAGCAG-3′ and (antisense) 5′-CTACCNGGGTATCTAAT-3′) was amplified using an optimized and standardized 16S-amplicon-library preparation protocol (Metabiote, GenoScreen). Briefly, 16S rDNA gene PCR was performed using 5 ng genomic DNA according to the manufacturer's protocol (Metabiote) using 192 bar-coded primers (Metabiote MiSeq Primers) at final concentrations of 0.2 µM and an annealing temperature of 50 °C for 30 cycles. The PCR products were purified using an Agencourt AMPure XP-PCR Purification system (Beckman Coulter), quantified according to the manufacturer's protocol, and multiplexed at equal concentrations. Sequencing was performed using a 300-bp paired-end sequencing protocol on an Illumina MiSeq platform (Illumina) at GenoScreen. Raw paired-end reads were subjected to the following process: (1) quality-filtering using the PRINSEQ-lite PERL script38 by truncating the bases from the 3′ end that did not exhibit a quality <30 based on the Phred algorithm; (2) paired-end read assembly

using FLASH39 (fast length adjustment of short reads to improve genome assemblies) with a minimum overlap of 30 bases and a 97% overlap identity; and (3) searching and removing both forward and reverse primer sequences using CutAdapt, with no mismatches allowed in the primers sequences. Assembled sequences for which perfect forward and reverse primers were not found were eliminated.

QUANTIFICATION AND STATISTICAL ANALYSIS

16S rDNA gene sequence analysis

The sequences were demultiplexed, quality-filtered using the 'quantitative insights into microbial ecology' (QIIME, version 1.8.0) software package (Caporaso et al., 2010), and the forward and reverse Illumina reads were joined using the fastq-join method (http://code.google.com/p/ea-utils). The sequences were assigned to OTUs using the UCLUST algorithm (Edgar, 2010) with a 97% threshold of pairwise identity and classified taxonomically using the Greengenes reference database (McDonald et al., 2012). Rarefaction was performed (30,000 sequences per sample) and used to compare the abundances of OTUs across samples.

Statistical analysis

Diabetes incidence was plotted according to the Kaplan-Meier method. Incidences between each group were compared with the log-rank test. Reported values are median +/− interquartile range as indicated. Comparison between each group was performed using the non-parametric Mann-Whitney U-test. P values < 0.05 were considered statistically significant. All data were analyzed using GraphPad Prism v6 software.

DATA AND SOFTWARE AVAILABILITY

The RNA-seq data reported in this paper is published in Mendeley Data (http://dx.doi.org/10.17632/4g2jdjxcff.1).

Figure 1

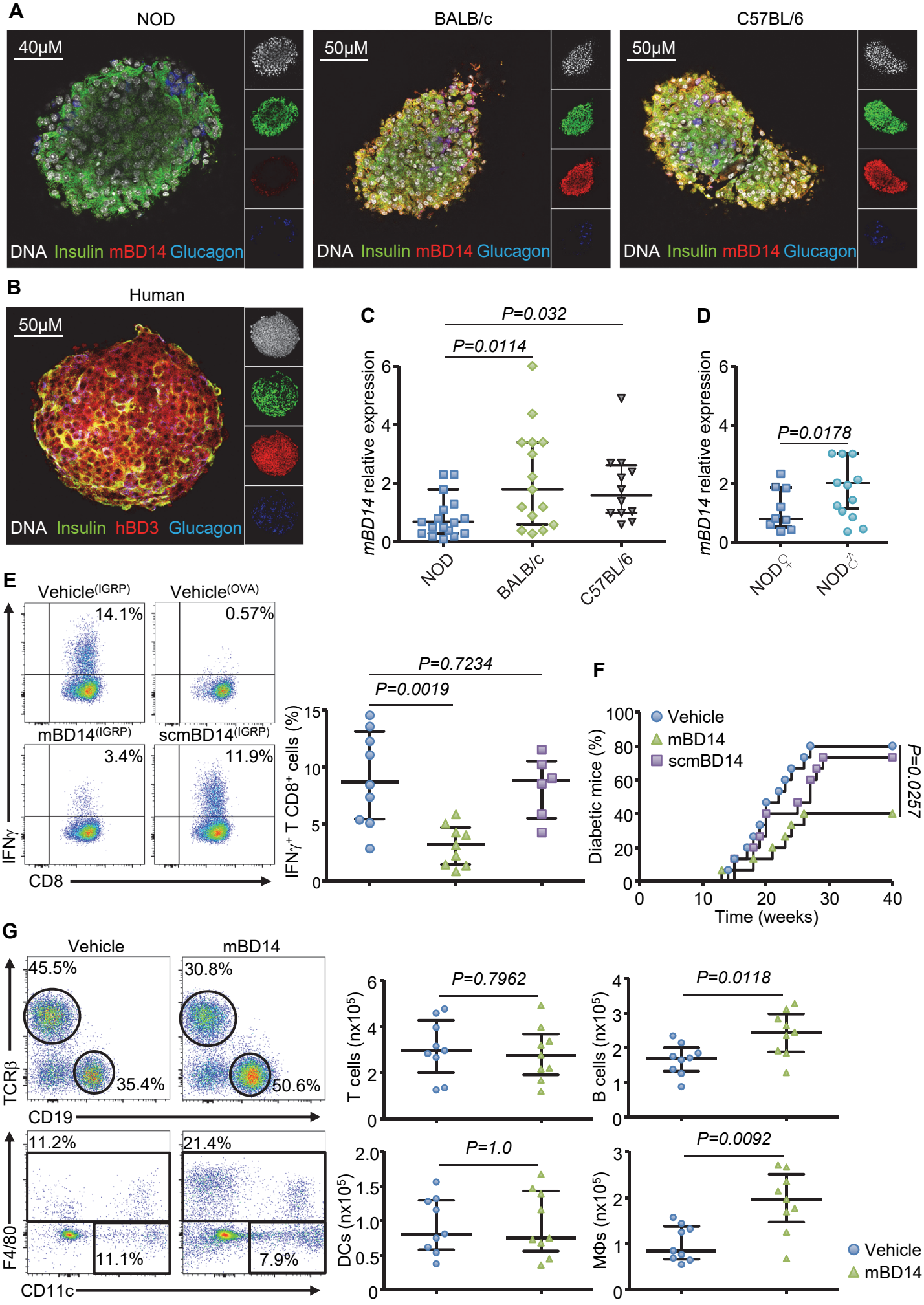
A
NOD
BALB/c
C57BL/6
40μM
50μM
50μM
DNA Insulin mBD14 Glucagon
DNA Insulin mBD14 Glucagon
DNA Insulin mBD14 Glucagon
B
Human
50μM
DNA Insulin hBD3 Glucagon
C
P=0.032
P=0.0114
mBD14 relative expression
NOD
BALB/c
C57BL/6
D
P=0.0178
mBD14 relative expression
NOD♀
NOD♂
E
Vehicle(IGRP)
Vehicle(OVA)
14.1%
0.57%
mBD14(IGRP)
scmBD14(IGRP)
3.4%
11.9%
IFNγ
CD8
P=0.7234
P=0.0019
IFNγ+ T CD8+ cells (%)
F
Vehicle
mBD14
scmBD14
Diabetic mice (%)
P=0.0257
Time (weeks)
G
Vehicle
mBD14
45.5%
35.4%
30.8%
50.6%
TCRβ
CD19
11.2%
11.1%
21.4%
7.9%
F4/80
CD11c
P=0.7962
T cells (nx10^5)
P=0.0118
B cells (nx10^5)
P=1.0
DCs (nx10^5)
P=0.0092
MΦs (nx10^5)
Vehicle
mBD14

Figure 2

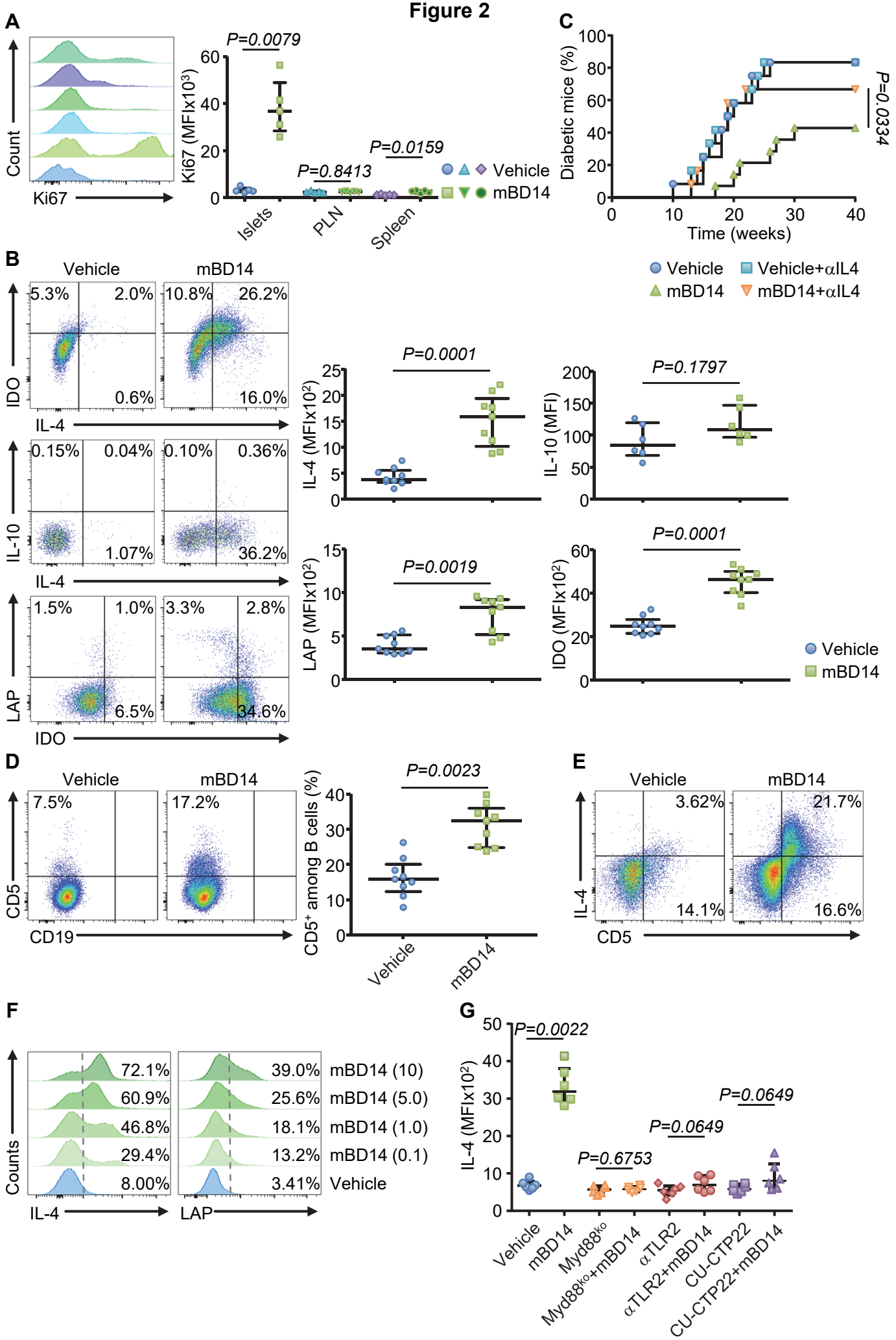
A
Count
Ki67
P=0.0079
Ki67 (MFIx10³)
P=0.8413
P=0.0159
Vehicle
mBD14
Islets
PLN
Spleen
C
Diabetic mice (%)
Time (weeks)
P=0.0334
B
Vehicle
mBD14
Vehicle
Vehicle+αIL4
mBD14
mBD14+αIL4
IDO
IL-4
5.3%
2.0%
0.6%
10.8%
26.2%
16.0%
IL-10
0.15%
0.04%
1.07%
0.10%
0.36%
36.2%
LAP
IDO
1.5%
1.0%
6.5%
3.3%
2.8%
34.6%
P=0.0001
IL-4 (MFIx10²)
P=0.1797
IL-10 (MFI)
P=0.0019
LAP (MFIx10²)
P=0.0001
IDO (MFIx10²)
Vehicle
mBD14
D
Vehicle
mBD14
CD5
CD19
7.5%
17.2%
P=0.0023
CD5⁺ among B cells (%)
Vehicle
mBD14
E
Vehicle
mBD14
IL-4
CD5
3.62%
21.7%
14.1%
16.6%
F
Counts
IL-4
LAP
72.1%
60.9%
46.8%
29.4%
8.00%
39.0%
25.6%
18.1%
13.2%
3.41%
mBD14 (10)
mBD14 (5.0)
mBD14 (1.0)
mBD14 (0.1)
Vehicle
G
IL-4 (MFIx10²)
P=0.0022
P=0.0649
P=0.0649
P=0.6753
Vehicle
mBD14
Myd88ko
Myd88ko+mBD14
αTLR2
αTLR2+mBD14
CU-CTP22
CU-CTP22+mBD14

Figure 3

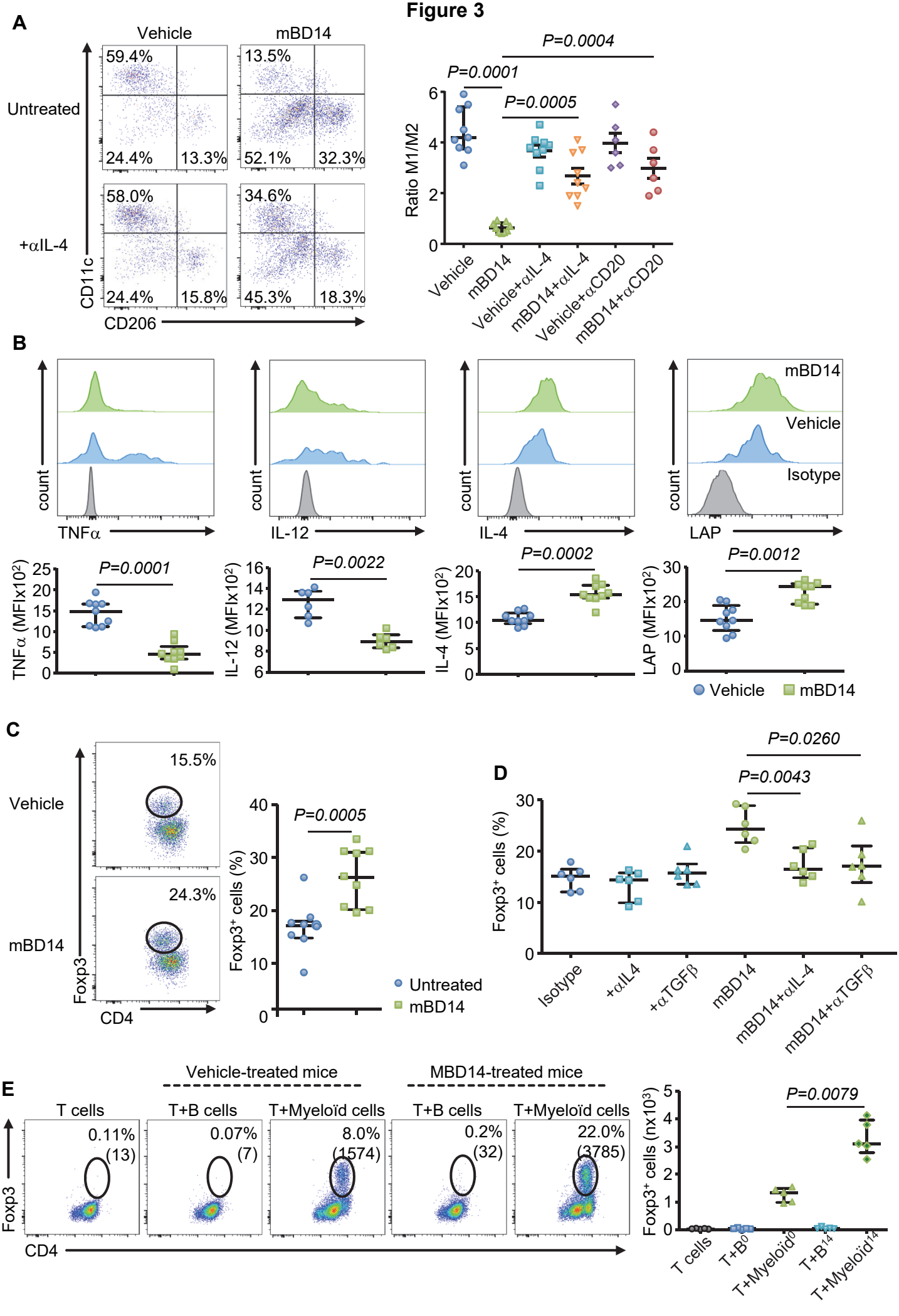
A
Vehicle
mBD14
Untreated
+αIL-4
59.4%
24.4%
13.3%
13.5%
52.1%
32.3%
58.0%
24.4%
15.8%
34.6%
45.3%
18.3%
CD11c
CD206
P=0.0004
P=0.0001
P=0.0005
Ratio M1/M2
Vehicle
mBD14
Vehicle+αIL-4
mBD14+αIL-4
Vehicle+αCD20
mBD14+αCD20
B
count
TNFα
IL-12
IL-4
LAP
mBD14
Vehicle
Isotype
P=0.0001
P=0.0022
P=0.0002
P=0.0012
TNFα (MFIx10²)
IL-12 (MFIx10²)
IL-4 (MFIx10²)
LAP (MFIx10²)
Vehicle
mBD14
C
Vehicle
mBD14
15.5%
24.3%
Foxp3
CD4
P=0.0005
Foxp3⁺ cells (%)
Untreated
mBD14
D
P=0.0260
P=0.0043
Foxp3⁺ cells (%)
Isotype
+αIL4
+αTGFβ
mBD14
mBD14+αIL-4
mBD14+αTGFβ
E
Vehicle-treated mice
MBD14-treated mice
T cells
T+B cells
T+Myeloïd cells
T+B cells
T+Myeloïd cells
0.11%
(13)
0.07%
(7)
8.0%
(1574)
0.2%
(32)
22.0%
(3785)
Foxp3
CD4
P=0.0079
Foxp3⁺ cells (nx10³)
T cells
T+B⁰
T+Myeloid⁰
T+B¹⁴
T+Myeloid¹⁴

Figure 4

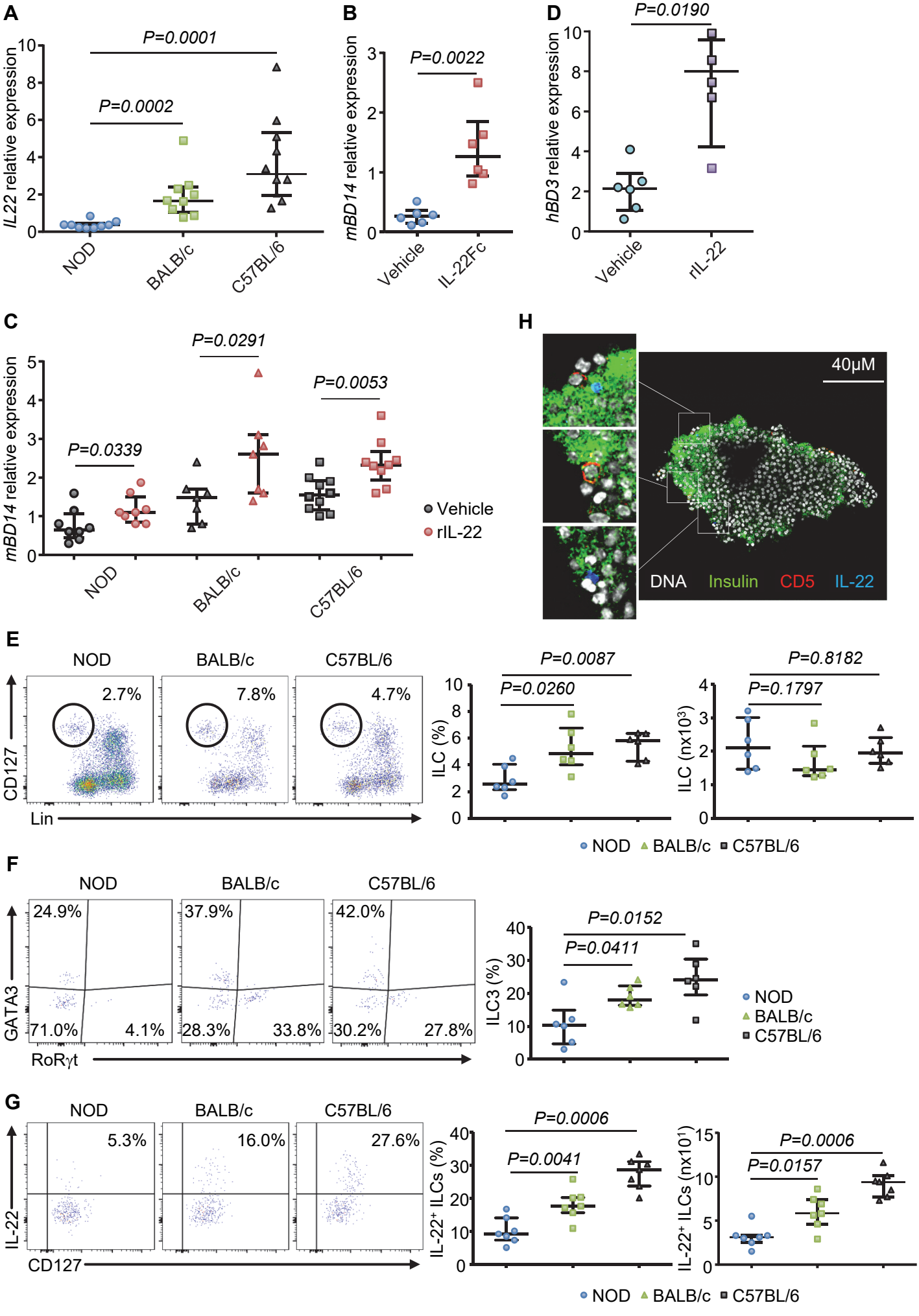
A
IL22 relative expression
P=0.0001
P=0.0002
NOD
BALB/c
C57BL/6
B
mBD14 relative expression
P=0.0022
Vehicle
IL-22Fc
D
hBD3 relative expression
P=0.0190
Vehicle
rIL-22
C
mBD14 relative expression
P=0.0291
P=0.0053
P=0.0339
NOD
BALB/c
C57BL/6
Vehicle
rIL-22
H
40μM
DNA
Insulin
CD5
IL-22
E
NOD
BALB/c
C57BL/6
2.7%
7.8%
4.7%
CD127
Lin
P=0.0087
P=0.0260
ILC (%)
P=0.8182
P=0.1797
ILC (nx10³)
NOD
BALB/c
C57BL/6
F
NOD
BALB/c
C57BL/6
24.9%
37.9%
42.0%
71.0%
4.1%
28.3%
33.8%
30.2%
27.8%
GATA3
RoRγt
P=0.0152
P=0.0411
ILC3 (%)
NOD
BALB/c
C57BL/6
G
NOD
BALB/c
C57BL/6
5.3%
16.0%
27.6%
IL-22
CD127
P=0.0006
P=0.0041
IL-22⁺ ILCs (%)
P=0.0006
P=0.0157
IL-22⁺ ILCs (nx10¹)
NOD
BALB/c
C57BL/6

Figure 5

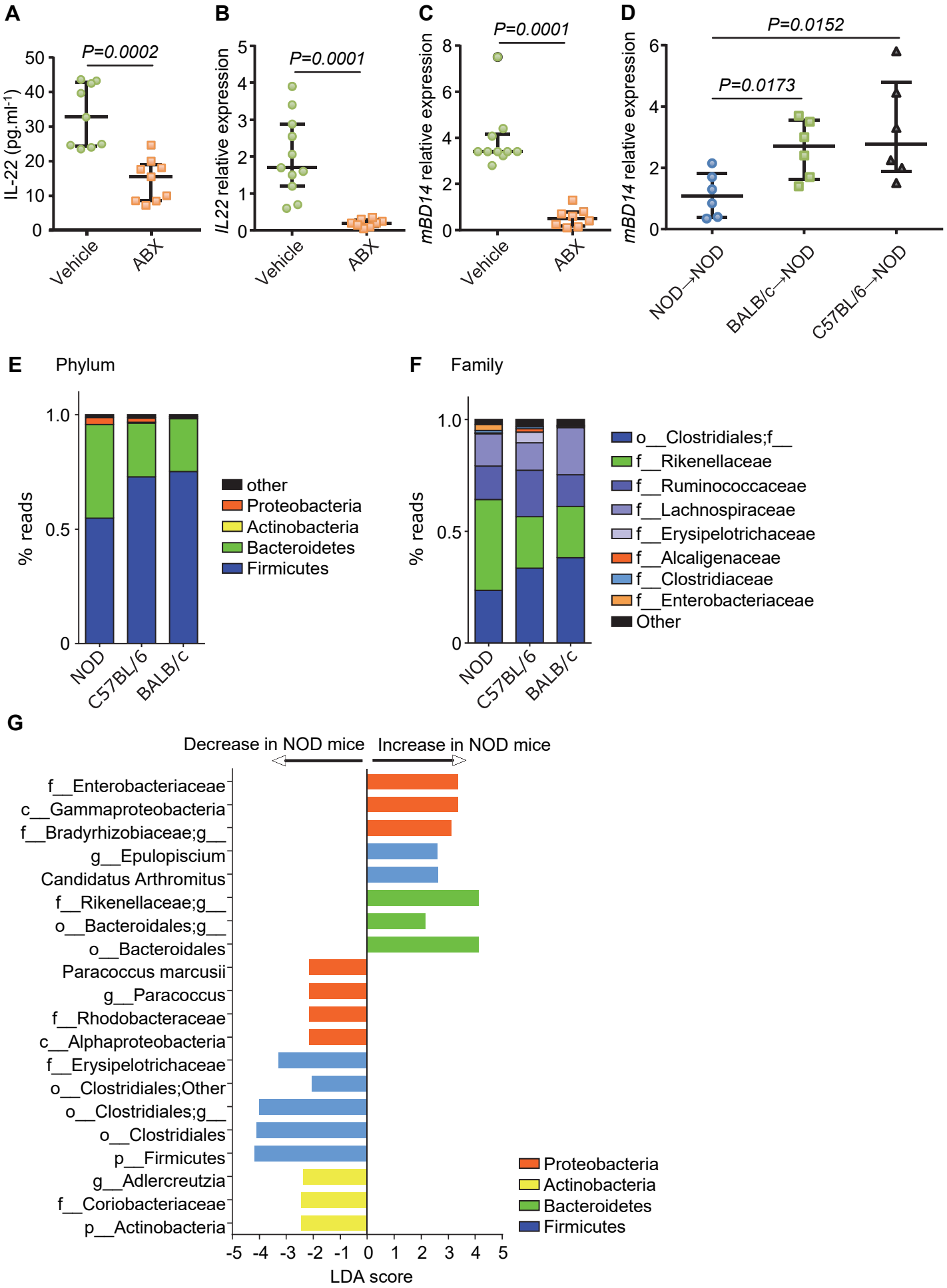
A
P=0.0002
IL-22 (pg.ml-1)
Vehicle
ABX
B
P=0.0001
IL22 relative expression
C
P=0.0001
mBD14 relative expression
D
P=0.0152
P=0.0173
mBD14 relative expression
NOD→NOD
BALB/c→NOD
C57BL/6→NOD
E
Phylum
% reads
NOD
C57BL/6
BALB/c
other
Proteobacteria
Actinobacteria
Bacteroidetes
Firmicutes
F
Family
o__Clostridiales;f__
f__Rikenellaceae
f__Ruminococcaceae
f__Lachnospiraceae
f__Erysipelotrichaceae
f__Alcaligenaceae
f__Clostridiaceae
f__Enterobacteriaceae
Other
G
Decrease in NOD mice
Increase in NOD mice
f__Enterobacteriaceae
c__Gammaproteobacteria
f__Bradyrhizobiaceae;g__
g__Epulopiscium
Candidatus Arthromitus
f__Rikenellaceae;g__
o__Bacteroidales;g__
o__Bacteroidales
Paracoccus marcusii
g__Paracoccus
f__Rhodobacteraceae
c__Alphaproteobacteria
f__Erysipelotrichaceae
o__Clostridiales;Other
o__Clostridiales;g__
o__Clostridiales
p__Firmicutes
g__Adlercreutzia
f__Coriobacteriaceae
p__Actinobacteria
LDA score
Proteobacteria
Actinobacteria
Bacteroidetes
Firmicutes

Figure 6

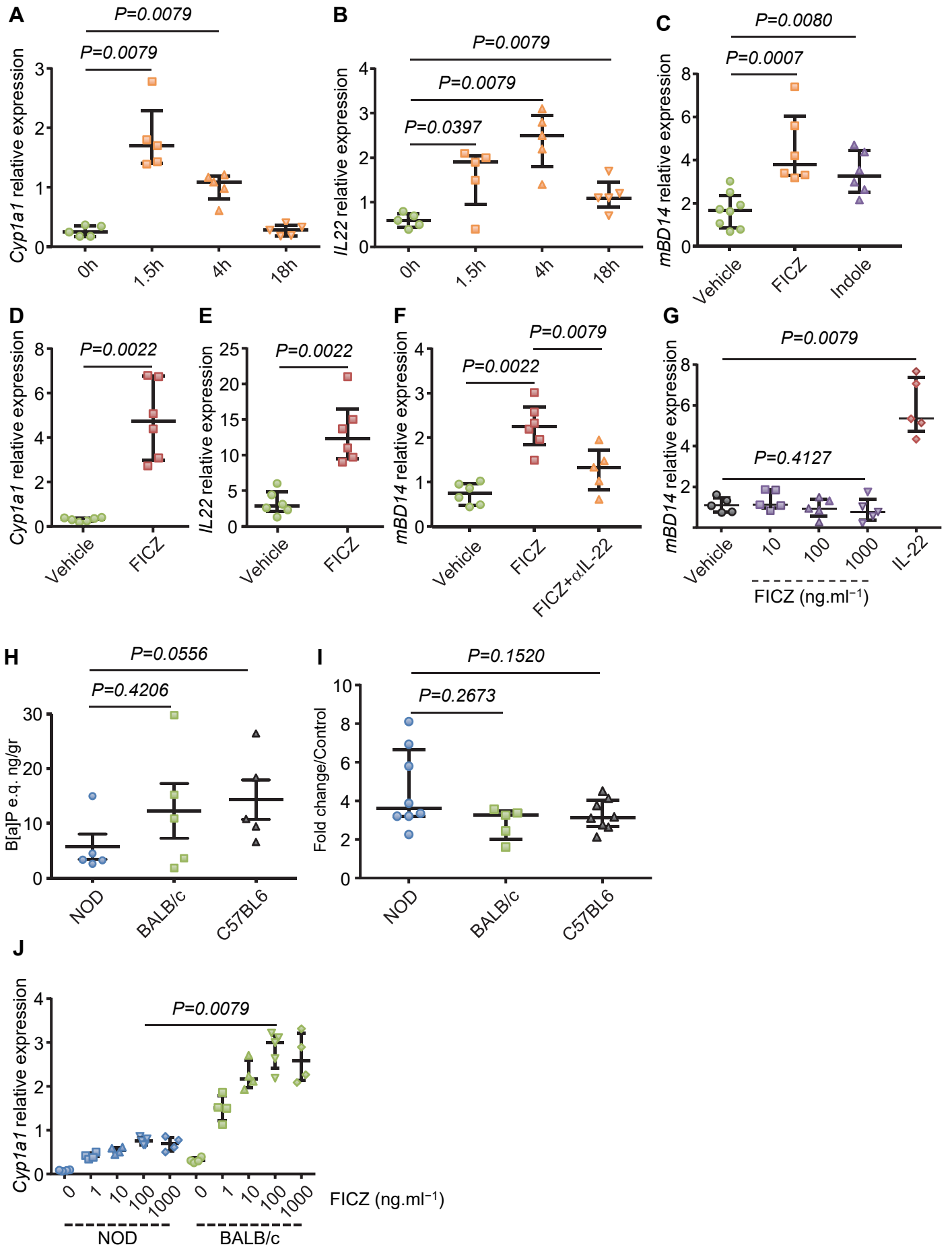
A
P=0.0079
P=0.0079
Cyp1a1 relative expression
0h
1.5h
4h
18h
B
P=0.0079
P=0.0079
P=0.0397
IL22 relative expression
C
P=0.0080
P=0.0007
mBD14 relative expression
Vehicle
FICZ
Indole
D
P=0.0022
Cyp1a1 relative expression
E
P=0.0022
IL22 relative expression
F
P=0.0079
P=0.0022
mBD14 relative expression
FICZ+αIL-22
G
P=0.0079
P=0.4127
10
100
1000
IL-22
FICZ (ng.ml⁻¹)
H
P=0.0556
P=0.4206
B[a]P e.q. ng/gr
NOD
BALB/c
C57BL6
I
P=0.1520
P=0.2673
Fold change/Control
J
P=0.0079
FICZ (ng.ml⁻¹)

Figure 7

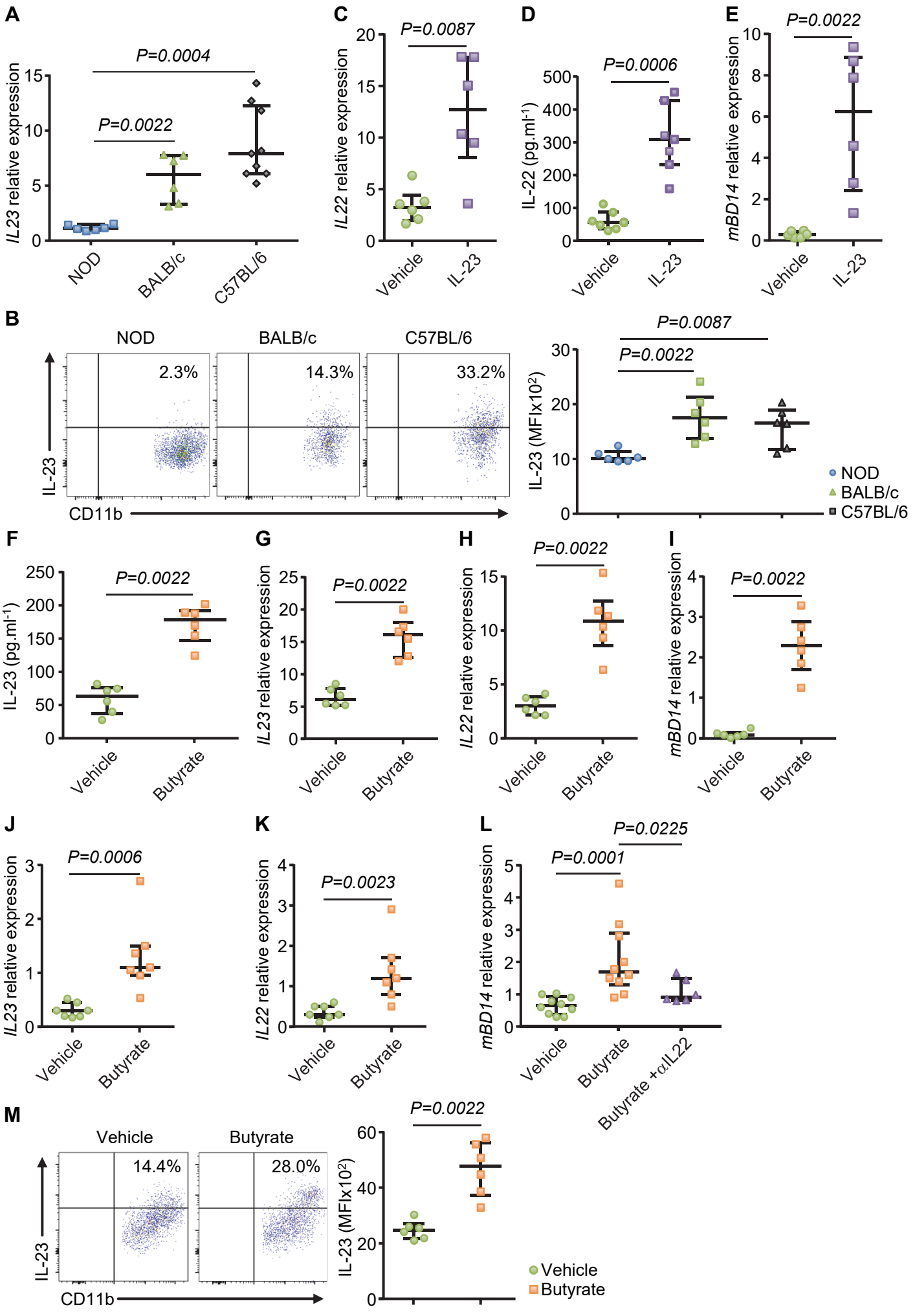
A
P=0.0004
P=0.0022
IL23 relative expression
NOD
BALB/c
C57BL/6
C
P=0.0087
IL22 relative expression
Vehicle
IL-23
D
P=0.0006
IL-22 (pg.ml-1)
E
P=0.0022
mBD14 relative expression
B
NOD
BALB/c
C57BL/6
2.3%
14.3%
33.2%
IL-23
CD11b
P=0.0087
P=0.0022
IL-23 (MFIx10²)
F
P=0.0022
IL-23 (pg.ml-1)
Butyrate
G
P=0.0022
IL23 relative expression
H
P=0.0022
IL22 relative expression
I
P=0.0022
mBD14 relative expression
J
P=0.0006
IL23 relative expression
K
P=0.0023
IL22 relative expression
L
P=0.0225
P=0.0001
mBD14 relative expression
Butyrate +αIL22
M
Vehicle
Butyrate
14.4%
28.0%
IL-23
CD11b
P=0.0022
IL-23 (MFIx10²)

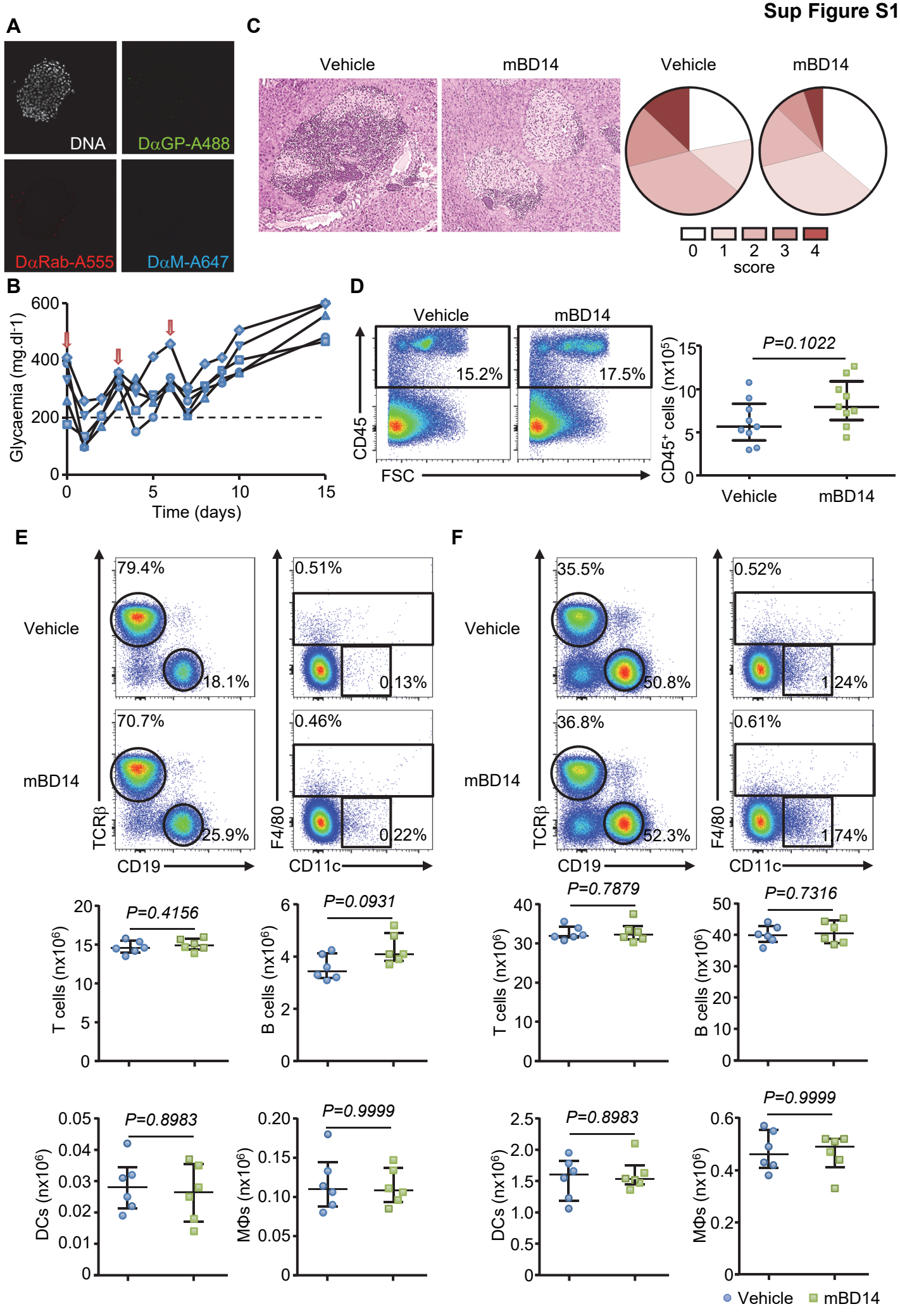
A
DNA
DαGP-A488
DαRab-A555
DαM-A647
C
Vehicle
mBD14
Vehicle
mBD14
0 1 2 3 4
score
B
Glycaemia (mg.dl-1)
Time (days)
D
Vehicle
mBD14
15.2%
17.5%
CD45
FSC
CD45+ cells (nx10^5)
P=0.1022
Vehicle
mBD14
E
Vehicle
mBD14
79.4%
18.1%
70.7%
25.9%
0.51%
0.13%
0.46%
0.22%
TCRβ
CD19
F4/80
CD11c
P=0.4156
P=0.0931
T cells (nx10^6)
B cells (nx10^6)
P=0.8983
P=0.9999
DCs (nx10^6)
MΦs (nx10^6)
F
Vehicle
mBD14
35.5%
50.8%
36.8%
52.3%
0.52%
1.24%
0.61%
1.74%
TCRβ
CD19
F4/80
CD11c
P=0.7879
P=0.7316
T cells (nx10^6)
B cells (nx10^6)
P=0.8983
P=0.9999
DCs (nx10^6)
MΦs (nx10^6)
Vehicle
mBD14

Sup Figure S2

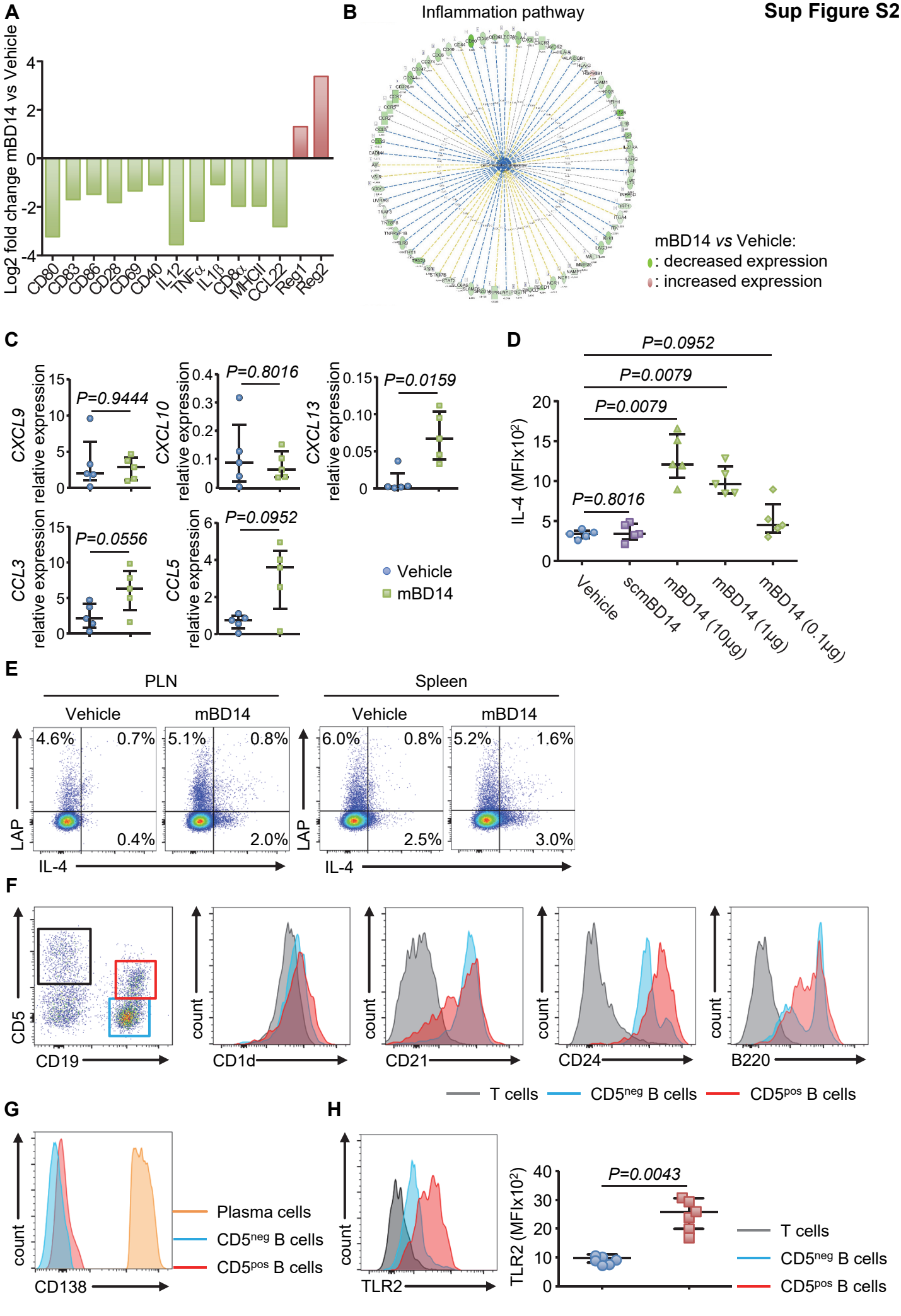

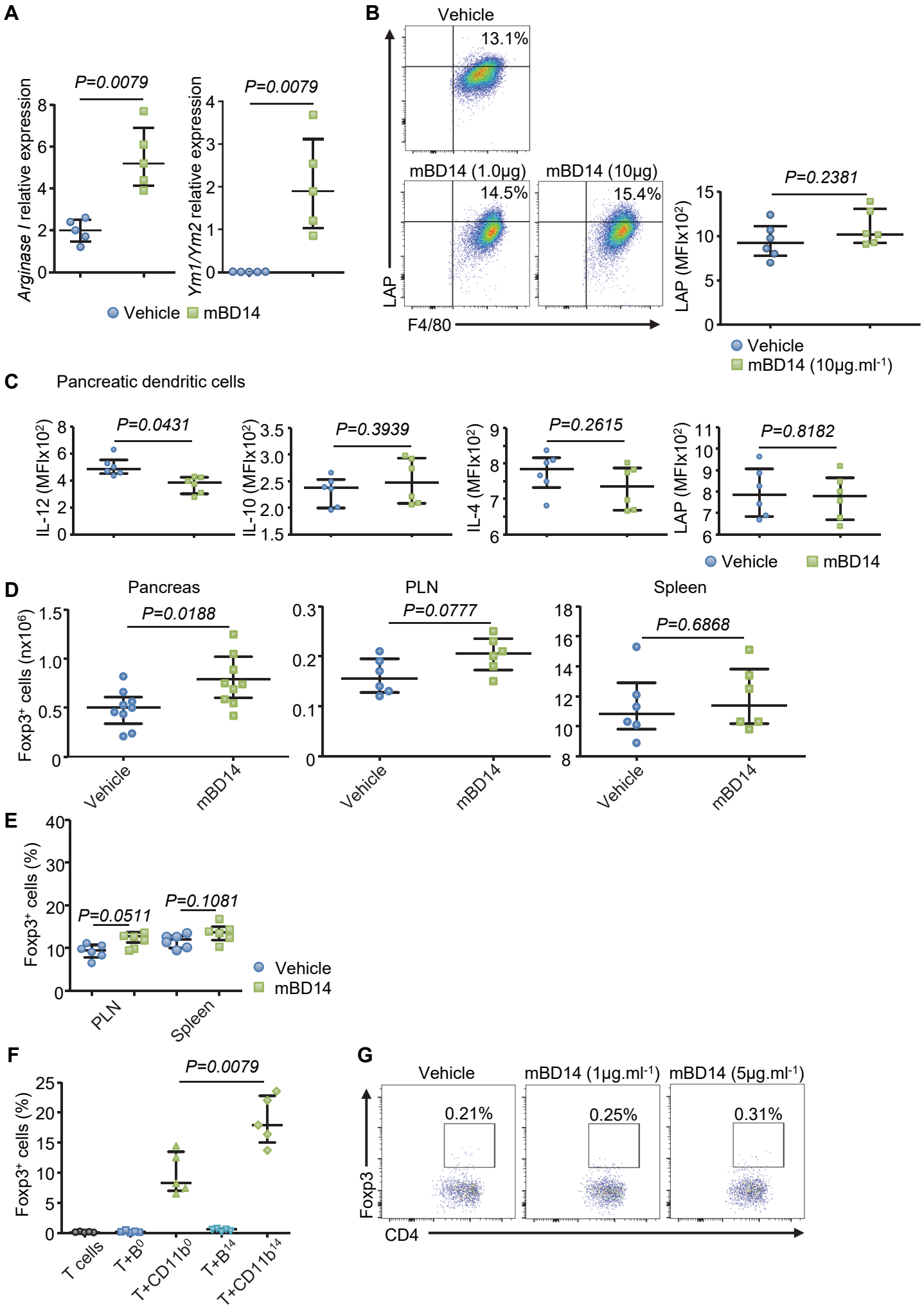
A
P=0.0079
P=0.0079
Arginase I relative expression
Ym1/Ym2 relative expression
Vehicle
mBD14
B
Vehicle
13.1%
mBD14 (1.0µg)
14.5%
mBD14 (10µg)
15.4%
LAP
F4/80
P=0.2381
LAP (MFIx10²)
Vehicle
mBD14 (10µg.ml⁻¹)
C
Pancreatic dendritic cells
P=0.0431
P=0.3939
P=0.2615
P=0.8182
IL-12 (MFIx10²)
IL-10 (MFIx10²)
IL-4 (MFIx10²)
LAP (MFIx10²)
Vehicle
mBD14
D
Pancreas
PLN
Spleen
P=0.0188
P=0.0777
P=0.6868
Foxp3⁺ cells (nx10⁶)
Vehicle
mBD14
E
P=0.0511
P=0.1081
Foxp3⁺ cells (%)
Vehicle
mBD14
PLN
Spleen
F
P=0.0079
Foxp3⁺ cells (%)
T cells
T+B⁰
T+CD11b⁰
T+B¹⁴
T+CD11b¹⁴
G
Vehicle
mBD14 (1µg.ml⁻¹)
mBD14 (5µg.ml⁻¹)
0.21%
0.25%
0.31%
Foxp3
CD4

Sup Figure S4

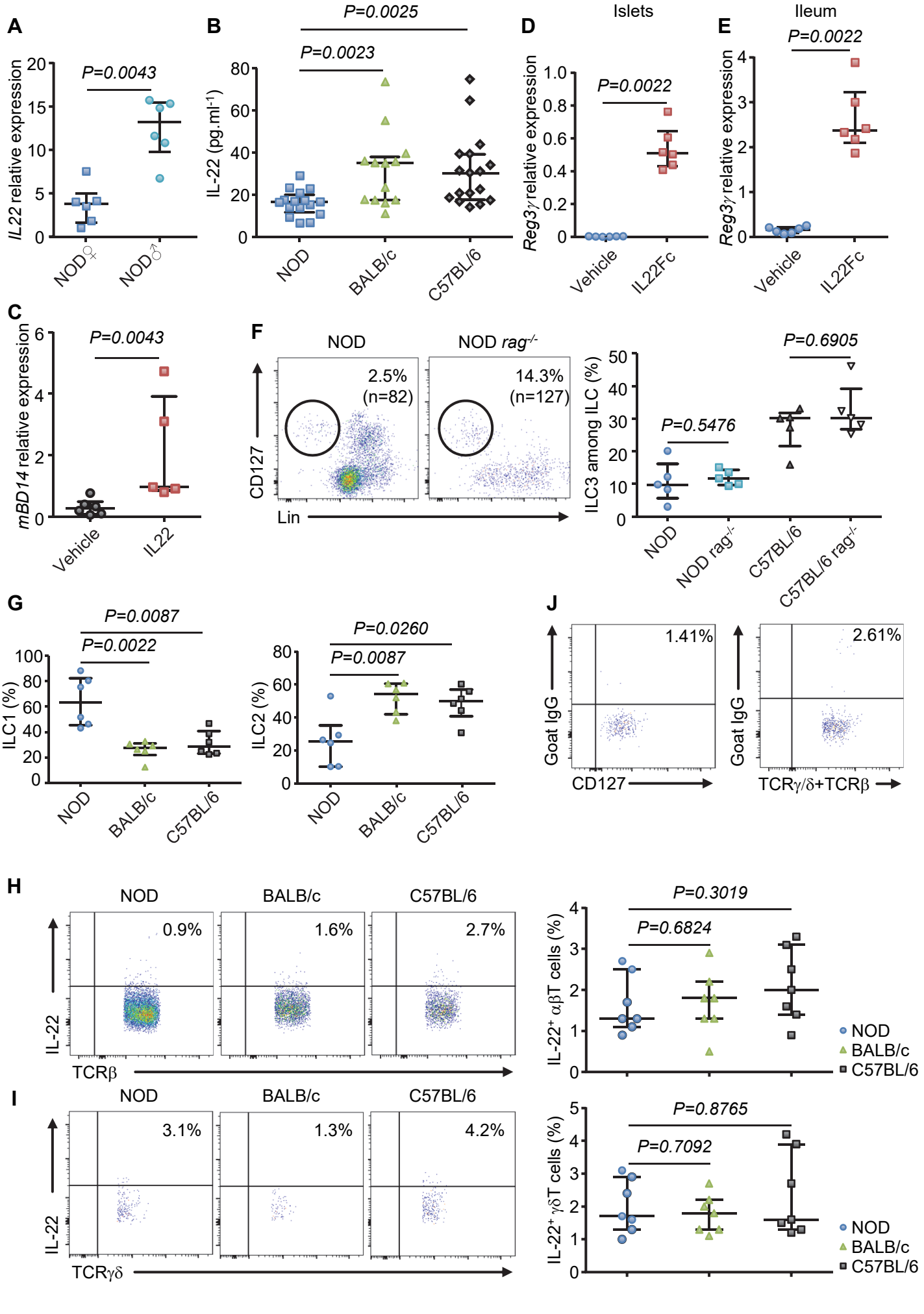

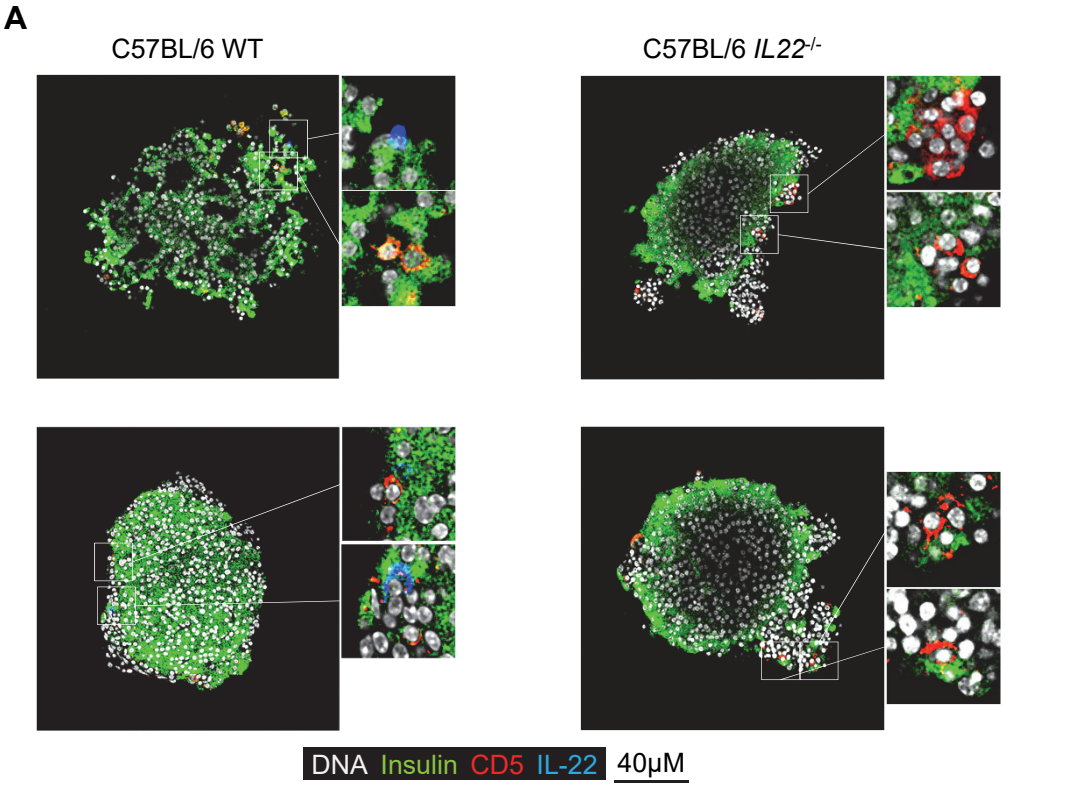
A
C57BL/6 WT
C57BL/6 IL22-/-
DNA Insulin CD5 IL-22 40µM

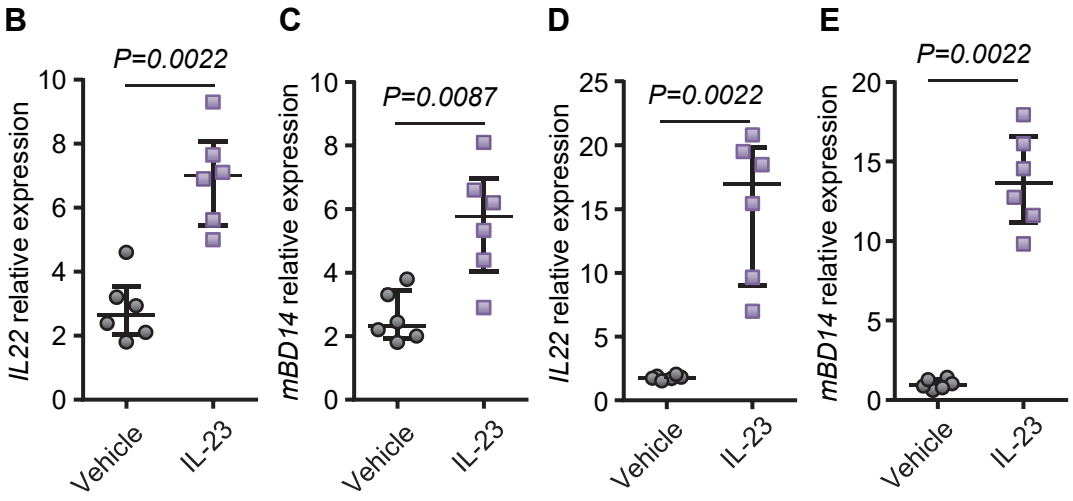
B
P=0.0022
IL22 relative expression
Vehicle
IL-23
C
P=0.0087
mBD14 relative expression
D
P=0.0022
IL22 relative expression
E
P=0.0022
mBD14 relative expression

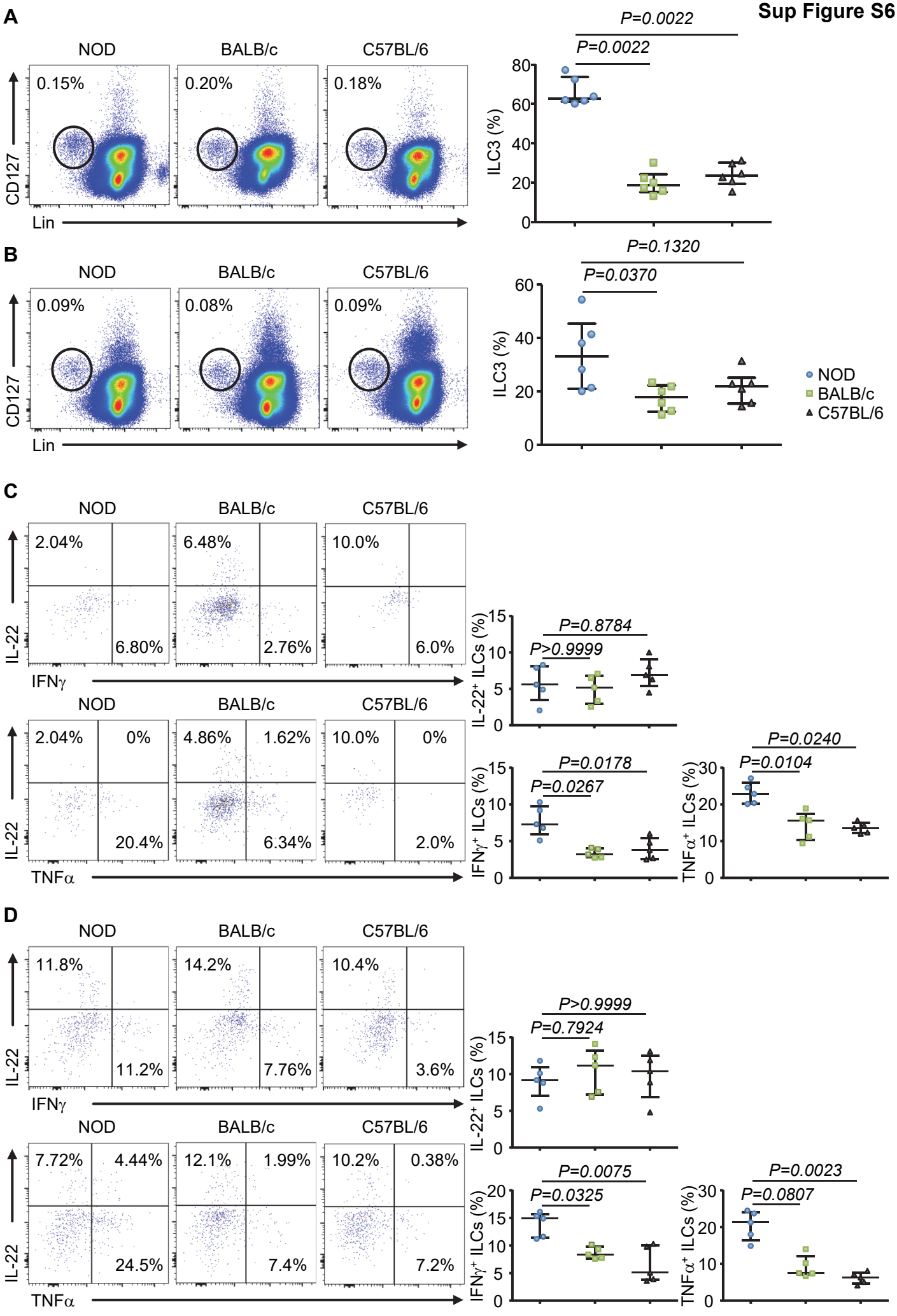
A
NOD
BALB/c
C57BL/6
0.15%
0.20%
0.18%
CD127
Lin
P=0.0022
P=0.0022
ILC3 (%)
B
0.09%
0.08%
0.09%
P=0.1320
P=0.0370
NOD
BALB/c
C57BL/6
C
2.04%
6.80%
6.48%
2.76%
10.0%
6.0%
IL-22
IFNγ
P=0.8784
P>0.9999
IL-22+ ILCs (%)
2.04%
0%
20.4%
4.86%
1.62%
6.34%
10.0%
0%
2.0%
TNFα
P=0.0178
P=0.0267
IFNγ+ ILCs (%)
P=0.0240
P=0.0104
TNFα+ ILCs (%)
D
11.8%
11.2%
14.2%
7.76%
10.4%
3.6%
P>0.9999
P=0.7924
7.72%
4.44%
24.5%
12.1%
1.99%
7.4%
10.2%
0.38%
7.2%
P=0.0075
P=0.0325
P=0.0023
P=0.0807

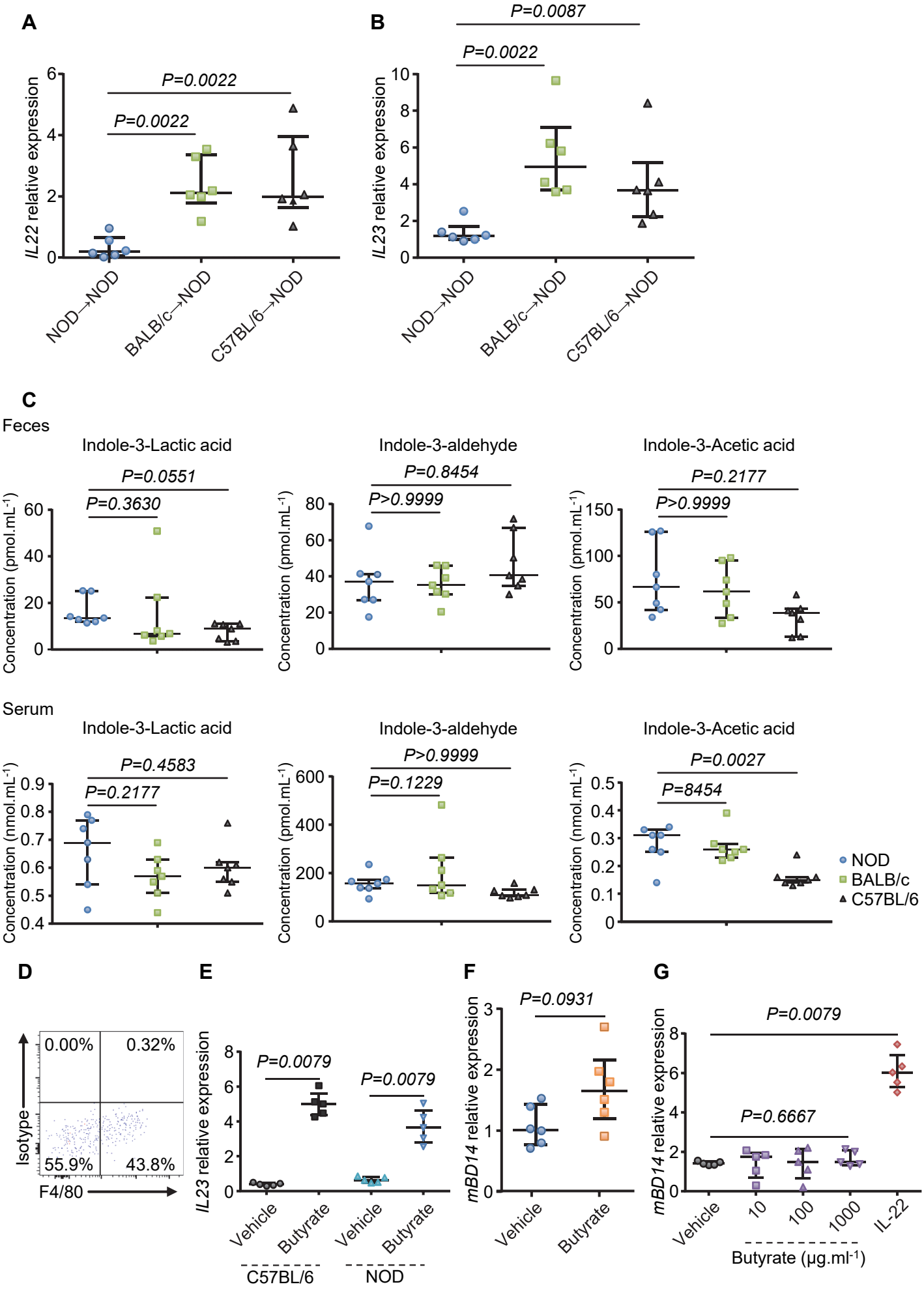
A
IL22 relative expression
P=0.0022
P=0.0022
NOD→NOD
BALB/c→NOD
C57BL/6→NOD
B
IL23 relative expression
P=0.0087
P=0.0022
C
Feces
Indole-3-Lactic acid
P=0.0551
P=0.3630
Indole-3-aldehyde
P=0.8454
P>0.9999
Indole-3-Acetic acid
P=0.2177
P>0.9999
Concentration (pmol.mL-1)
Serum
Indole-3-Lactic acid
P=0.4583
P=0.2177
Indole-3-aldehyde
P>0.9999
P=0.1229
Indole-3-Acetic acid
P=0.0027
P=8454
Concentration (nmol.mL-1)
NOD
BALB/c
C57BL/6
D
Isotype
F4/80
0.00%
0.32%
55.9%
43.8%
E
IL23 relative expression
P=0.0079
P=0.0079
Vehicle
Butyrate
C57BL/6
NOD
F
mBD14 relative expression
P=0.0931
G
mBD14 relative expression
P=0.0079
P=0.6667
10
100
1000
IL-22
Butyrate (µg.ml-1)

Supplementary Figure legends

Figure S1. Related to Figure 1. Expression of mBD14 and its effect of on immune cell population in female NOD mice. (A) Isolated islets from female BALB/c were stained with anti-guinea pig-AlexaFluor488, anti-mouse-Alexa647, anti-rabbit-AlexaFluor555 pAbs and DAPI (Invitrogen). Data are representative of 6 independent experiments. (B) Diabetic NOD mice (glycemia >200 $mg.ml^{-1}$)) were treated (red arrow) with mBD14 (10 µg/mouse) and glycemia was followed, n=5 mice. (C) Eight-weeks-old NOD mice received one injection of mBD14 or scmBD14 (10 µg) per week during two weeks and histological scoring of insulitis was performed at 25 weeks of age on pancreatic sections stained with hematoxylin-eosin. Grade 0, no infiltration; grade 1, <25% lymphocytic infiltration; grade 2, 25-50% islet lymphocytic infiltration, grade 3, >50-75% islet lymphocytic infiltration and grade 4, >75% islet lymphocytic infiltration. Data are representative of two independent experiments with 5 independent mice per group. (D-F) Immune cell populations in the pancreatic islets (D), lymph nodes (E) and spleen (F) from NOD mice treated with mBD14 or vehicle (d–4) were determined by flow cytometry. Data are the frequency and number of $CD45^+$ cells (D) or of gated cells ($CD19^+$ B cell, $TCR\beta^+$ T cell, $F4/80^-$ $CD11c^+$ DC and $F4/80^+$ $CD11b^+$ macrophage) among the $CD45^+$ population (E, F). Data are representative or are the median +/– interquartile range of 6 to 9 independent mice per group.

Figure S2. Related to Figure 1 and 2. (A-B) RNA-seq analysis of pancreatic islets from 10-wk-old female NOD mice treated with mBD14 (10 µg/mouse) or vehicle (d–5), n=3 mice per group. (A) Log2 gene expression fold changes between mBD14-treated mice *v.s.* vehicle-treated mice. (B) The Ingenuity pathway analysis (IPA, Qiagen) Tool was used to generate the most significant canonical pathways impacted by mBD14 treatment. Color intensity indicates the degree of upregulation (red) or downregulation (green) comparing mBD14- *v.s.* vehicle-

treated mice. Solid lines represent direct interactions and dashed lines indirect interactions. (C-H) Analysis of B cell population after mBD14 treatment in female NOD mice. (C) Expression of chemokine mRNAs was analyzed by RT-qPCR in pancreatic islets from NOD mice treated with mBD14 or vehicle (d–4). Data are the median +/– interquartile range of 5 independent mice per group. (D, E) NOD mice were treated with mBD14 (10 µg/mouse in E or growing dose in D) or vehicle (d–3). B cells ($CD19^+$ $CD11b^–$) from pancreatic islets (D), lymph nodes and spleen (E) were analyzed by flow cytometry. Cells were incubated for 5 h in the presence of a protein transport inhibitor cocktail before staining. Results show the frequency of positive cells or the MFI of IL-4 among B cell population as indicated. Data are representative (E) or are the median +/– interquartile range (D) of 5 independent mice per group. (F-H) B cells ($CD45^+$ $CD19^+$ $CD11b^–$) from the pancreatic islets of mBD14-treated NOD mice were analyzed by flow cytometry for surface expression of the indicated markers. Data are representative (F, G) or are the median +/– interquartile range (H) of 6 independent mice.

Figure S3. Related to Figure 3. Effect of mBD14 on macrophages and dendritic cells and on Treg cell induction. (A) Expression of arginase I and Ym1/Ym2 mRNAs was analyzed by RT-qPCR in pancreatic macrophages magnetically isolated ($F4/80^+$) from NOD mice treated with mBD14 or vehicle (d–4). Data are the median +/– interquartile range of 5 independent mice per group. (B) Bone-marrow derived macrophages were differentiated in presence of M-CSF during 8 days and then treated with vehicle or mBD14 at the indicated dose for 24 h. Then cells were stained for LAP expression on $CD11b^+$ $F4/80^+$ cells. Data are representative and are the median +/– interquartile range of 6 independent experiments. (C) Cytokine intracellular expression in pancreatic dendritic cells was analyzed in NOD mice treated with mBD14 or vehicle (d–4). Cells were incubated for 5 h in the presence of LPS and a protein transport inhibitor cocktail before staining. Results show the MFI of indicated marker among $CD11b^+$

$CD11c^+$ $F4/80^-$ mice. Data are representative and are the median +/– interquartile range of 6 independent mice per group. (D, E) Regulatory T cells were analyzed in pancreatic islets, lymph nodes and spleen from NOD mice treated with mBD14 or vehicle (day–10). Results show the number (D) and the frequency (E) of Treg cells ($Foxp3^+$) among the $CD4^+$ T cell population. Data are representative and are the median +/– interquartile range of 6 independent mice per group. (F) Pancreatic myeloid cells ($CD11b^+$) or B cells ($CD19^+$) were isolated from NOD mice treated with vehicle (^{0}) or mBD14 (^{14}) (day–4) and cultured for 4 days with naïve ($CD62L^+$) BDC2.5 $CD4^+$ T cells devoid in Treg cells ($CD25^-$). Treg cell induction was analyzed by flow cytometry. Data show the frequency of Treg cells ($Foxp3^+$ $CD25^+$) among the CD4 T cell population. Data are the median +/– interquartile range of 5 independent experiments with 4 mice pooled per group in each experiment. (G) Naïve BDC2.5 T cells devoid in Treg cells were cultured for 4 days in presence of mBD14 at the indicated doses. Treg cell induction was analyzed by flow cytometry. Data show the frequency of Treg cells ($Foxp3^+$ $CD25^+$) among the CD4 T cell population. Data are representative of 3 independent experiments.

Figure S4. Related to Figure 4. Effect of IL-22 on pancreatic expression of mBD14. (A) Expression of IL22 mRNA was analyzed by RT-qPCR in islets from female and male NOD mice. Data are the median +/– interquartile range of 6 independent mice per group. (B) Level of IL-22 in the serum of female mice was determined by ELISA. Data are the median +/– interquartile range of a minimum of 13 independent mice per group. (C) Expression of mBD14 mRNA in Min6 cells was analyzed by RT-qPCR treated with vehicle or rmIL-22 (200 $ng.ml^{-1}$) for 12 h. Data are the median +/– interquartile range of 5 independent experiments. (D, E) Expression of Reg3γ mRNA was analyzed by RT-qPCR in islets and ileum from female NOD mice treated with vehicle or IL-22Fc (100 µg/mouse) for 3 h. Data are the median +/– interquartile range of 6 independent mice per group. (F, G) Innate lymphoid cells (ILCs) were

analyzed in the islets from the indicated mouse strains. Data show the frequency of ILCs ($CD127^+$ $CD90^+$ Lin (CD5, CD19, CD11b, $CD11c)^-$) among $CD45^+$ immune cells and of ILC3s ($RoR\gamma t^+$ $GATA3^-$) among ILCs in WT and *Rag*$^{-/-}$ mice (F) and the frequency of ILC1s ($GATA3^-$ $RoR\gamma t^-$) and ILC2s ($GATA3^+$ $RoR\gamma t^-$) among ILC population (G). Data are representative and are the median +/– interquartile range of 6 independent mice per group. (H-I) To determine IL-22 intracellular expression, cell suspension from the islets was cultured for 5 h with rmIL-23 plus PMA/ionomycin in presence of a protein transport inhibitor cocktail before staining. Data show the frequency of IL-22^+ cells among the α/β or the γ/δ T cell populations. Data are representative and are the median +/– interquartile range of 7 independent mice per group. (J) Cells were treated as in I before staining with goat IgG as control isotype for IL-22 staining. Data show the frequency of goat IgG^+ cells among the ILCs (left panel) or α/β plus γ/δ T cells (right panel). Data are representative of 4 independent experiments.

Figure S5. Related to Figure 4. (A) Pancreatic islets from C57BL/6 WT or *IL22*$^{-/-}$ female mice were cultured for 5 h in presence of rmIL23 plus PMA/ionomycin in presence of a protein transport inhibitor cocktail and stained for insulin (green), CD5 (red), IL-22 (blue) and DNA (grey). Data are representative of 3 independent experiments. (B-E) mRNA expression of IL22 and mBD14 was determined in pancreatic islets (B, C) and ileum (D, E) from C57BL/6 $Rag^{-/-}$ female mice treated with rmIL-23 (2 µg, i.p., h–2). Data are the median +/– interquartile range of 6 independent mice per group.

Figure S6. Related to Figure 4. Analysis of innate lymphoid cells in lymphoid tissues and small intestine. (A-B) Innate lymphoid cells (ILCs) were analyzed in the pancreatic (A) and mesenteric (B) lymph nodes from the indicated mouse strains. Data show the frequency of ILCs ($CD127^+$ $CD90^+$ Lin (CD5, CD19, CD11b, $CD11c)^-$) among $CD45^+$ immune cells and the

frequency of ILC3s (RoRγt^{+} GATA3^{-}) among the ILC population. Data are representative and are the median +/– interquartile range of 4 to 6 independent mice per group. (C-D) Analysis of cytokine expression in ILCs from lymphoid tissues. Cell suspension from the pancreatic (C) or mesenteric (D) LN was cultured for 5 h with rmIL-23 plus PMA/ionomycin in presence of a protein transport inhibitor cocktail before intracellular staining for IL-22, IFNγ and TNFα expression. Data show the frequency of cytokine^{+} cells among the ILC population. Data are representative and are the median +/– interquartile range of 5 independent mice per group.

Figure S7. Related to Figure 5-7. Effect of gut microbiota transfer on IL22 and IL23 expression in the pancreatic islets. (A–B) Six-weeks-old NOD mice were transferred with gut microbiota from the different mouse strains (→). Seven days later mRNA expression of IL22 (A) and IL23 (B) in pancreatic islets was determined by RT-qPCR. Data are the median +/– interquartile range of 6 independent mice per group. (C) Composition in AHR ligands in the serum and feces from 10-wk-old female mice. AHR ligand level was determined by a specific method using HPLC-coupled to high resolution mass spectrometry. Data are the median +/– interquartile of 7 independent mice per group. (D–G) Expression of IL-23 in various cells and tissues and effect of butyrate on mBD14 expression. (D) Cell suspension from the pancreatic islets of BALB/c mice was cultured for 5 h in presence of LPS and a protein transport inhibitor cocktail before staining with anti-mouse IgG1 (isotype control for anti-IL23 mAb). Results show the frequency of gated cells in the CD11b+ CD19– population. Data are representative of 6 independent experiments. (E) C57BL/6 and NOD bone-marrow derived macrophages were differentiated in presence of M-CSF for 8 days, then activated with LPS (100 ng.ml–1) for 2 h and subsequently treated with butyrate (1 mg.ml–1) for 22 h. Expression of IL23 mRNA was determined by RTqPCR. Data are the median +/– interquartile range of 5 independent experiments. (F) mRNA expression of mBD14 was determined in pancreatic islets from NOD

mice treated with butyrate (1 mg/mouse, i.p.) daily for 5 days. Data are the median +/– interquartile of 6 independent mice per group. (G) Min6 cells were treated with growing doses of butyrate or IL-22 (200 ng.ml–1) for 24 h. The expression of mBD14 mRNA was determined by RT-qPCR. Data are the median +/– interquartile of 5 independent experiments.